Aus der Medizinischen Universitätsklinik und Poliklinik Tübingen, Abteilung Innere Medizin I

(Schwerpunkt: Gastroenterologie, Gastrointestinale Onkologie, Hepatologie, Infektiologie und Geriatrie)

Haprolid inhibits tumor growth of hepatocellular carcinoma through Rb/E2F and Akt/mTOR inhibition

Inaugural-Dissertation

zur Erlangung des Doktorgrades

der Medizin

der Medizinischen Fakultät

der Eberhard Karls Universität

zu Tübingen

vorgelegt von

Xing, Jun

2019

Dekan: Professor Dr. I. B. Autenrieth

1. Berichterstatter: Professor Dr. R. R. Plentz

2. Berichterstatter: Professor Dr. U. Lauer

Tag der Disputation: 09.12.2019

Contents

Abbreviations List

ABC	avidin-biotin complex
ADP	adenosine diphosphate
ALD	alcoholic liver disease
BCLC	Barcelona Clinic Liver Cancer
CDK	cyclin-dependent kinase
CT	computed tomography
DAB	3,3'-diaminobenzidine
DMSO	dimethyl sulfoxide
EGF	epidermal growth factor
EMT	epithelial-mesenchymal transition
FACS	fluorescence-activated cell sorting
FBS	fetal bovine serum
FGF	fibroblast growth factor
FoxO	Forkhead Box O
GAP	GTPase-activating protein
GPCR	G protein-coupled receptors
GSK3	glycogen synthase kinase 3
HCC	hepatocellular carcinoma
HDF	human dermal fibroblast
HR-ESI-MS	high-resolution electrospray ionisation mass spectrometry
HRP	horseradish peroxidase
IC50	concentration for 50% of maximal inhibition
IGF	insulin-like growth factor
IHC	immunohistochemistry
LR	liver resection
MAPK	mitogen-activated protein kinase

MRI	magnetic resonance imaging
mTOR	mammalian target of rapamycin
MWA	microwave ablation
NAFLD	non-alcoholic fatty liver disease
OLT	orthotopic liver transplantation
PARP	poly (ADP ribose) polymerase
PDGF	platelet-derived growth factor
PDK1	protein kinase 1
PDS	programmed cell death
PH	Pleckstrin homology
PI	propidium iodide
PKB	protein kinase B
PS	phospholipid phosphatidylserine
RFA	radiofrequency ablation
RTK	receptor tyrosine kinases
S6	ribosomal protein S6
S6K	ribosomal protein S6 kinase
SBRT	stereotactic body radiation therapy
TACE	transarterial chemoembolization
TARE	transarterial radioembolization
TSC2	tuberous sclerosis complex 2
VEGF	vascular endothelial growth factor
WST-1	water soluble tetrazolium salts

1. Introduction

1.1 Hepatocellular Carcinoma

Hepatocellular carcinoma (HCC) is one of the most commonly diagnosed cancers and the leading causes of cancer death worldwide [1]. Over the past 30 years, HCC is one of the few neoplasms with a steady increasing incidence and mortality [2] and these trends are expected to remain through 2030 [3]. Almost half of all patients with HCC are diagnosed at advanced stage when curative treatments are not applicable [4]. There are major unmet needs to discover novel palliative therapeutic approaches for the management of HCC.

1.1.1 Epidemiology

Liver cancer is the fifth most common cancer and the third most frequent cause of cancer-related death globally in 2018, with 841,080 new cases and 781,631 deaths per year, accounting for 8.2% of all cancers [5]. HCC represents approximately 90% of all cases of primary liver cancers and constitutes a major global health burden [2, 6]. The pattern of HCC occurrence shows a significant geographical imbalance, with the highest incidence rates in Eastern Asia (more than 50% of the cases occurring in China) followed by Micronesia and Northern Africa [5]. The incidence of HCC increases progressively with advancing age in all populations. HCC has a strong male preponderance, rates of both incidence and mortality are 2 to 3 times higher among men in its worldwide distribution [1, 5].

1.1.2 Aetiology and Risk factors

1.1.2.1 Hepatitis B or Hepatitis C, viral infection has been linked to be the highest risk factor for developing HCC. In Africa and Eastern Asia, the largest

attributable fraction is caused by hepatitis B virus (HBV) infection (66%), whereas in the Western world less than 20% of cases can be attributed to hepatitis B, while chronic hepatitis C infection appears to be the major risk factor [7]. Worldwide, HBV infection contributes to approximately 33% of HCC cases and most infections were acquired via perinatal and early horizontal transmission. Universal vaccination of newborns has led to a marked decline in HCC incidence compared with the pre-vaccination era. Meanwhile, approximately 21% of HCC cases can be attributed to HCV infection globally [7].

1.1.2.2 Alcohol abuse, excessive alcohol consumption is an independent risk factor for HCC. Alcohol-use disorder is one of the leading causes of cirrhosis, which in turn is linked with an increased risk of HCC [8]. The proportion of HCC which is attributable to alcoholic liver disease (ALD) has been constant, between 20% and 25% [9].

1.1.2.3 NAFLD, Obesity and Diabetes, the sharp growth in the prevalence of obesity and diabetes has resulted in an increasing population of patients with NAFLD [10]. The global prevalence of NAFLD is estimated at 25.2% and it is likely to continue increasing [11]. Patients with NAFLD can progress to fibrosis, cirrhosis and, eventually, HCC [12]. These patients are expected to drive the HCC epidemic in developed regions [13-15]. Type 2 diabetes has been linked with an increased risk of liver cancer, usually in patients who also have other risk factors such as heavy alcohol use and/or chronic viral hepatitis. Diabetes and obesity are the strongest metabolic factors associated with HCC [16].

1.1.2.4 Aflatoxins, aflatoxins are metabolites derived from fungal contaminations of staple foodstuffs preferentially in tropical and subtropical

regions. Aflatoxin B1 is the most potent experimental hepatocarcinogen and dietary exposure to aflatoxin B1 is considered to be an important co-factor for HCC development in parts of Africa and Asia [17]. Epidemiologic and molecular studies have demonstrated a strong correlation between aflatoxin B1 exposure, TP53 gene mutations (codon 249) and incidence of HCC, especially in HBV-infected individuals [18].

1.1.2.5 Certain rare diseases, diseases that increase the risk of HCC include:

Wilson disease

Haemochromatosis

Tyrosinemia

Alpha1-antitrypsin deficiency

Porphyria cutanea tarda

Glycogen storage diseases

1.1.2.6 Cirrhosis, cirrhosis is characterized by a destruction of liver cells and an increase in fibrous tissue which leads to an exhaustion of the liver regenerative capacity and the development of cancerous nodules. HCC predominantly arises in the context of cirrhosis and cirrhosis is present in 70% to 90% of HCC cases [19]. The main causes of cirrhosis in developed countries are alcohol abuse and non-alcoholic fatty liver disease (NAFLD), while HBV infection is the primary cause in China and other Asian countries [11]. Overall, one-third of cirrhotic patients will develop HCC during their lifetime [20].

1.1.3 Symptoms, Diagnosis and Treatments

1.1.3.1 Symptoms, clinical presentation of HCC can vary from asymptomatic patients to patients presenting variable symptoms such as weight loss, fatigue,

loss of appetite, pain, jaundice, ascites, splenomegaly, variceal bleeding, anasarca, hepatic encephalopathy, lethargy, diarrhoea, paraneoplastic symptoms, cutaneous manifestations, and abnormal laboratory values. In fact, many of these symptoms are more likely to be caused by other conditions such as chronic liver disease and cirrhosis instead of tumor itself.

1.1.3.2 Diagnosis, the diagnosis of HCC is based on histological analysis, contrast-enhanced imaging findings including ultrasound, multiphase computed tomography (CT) and multiphase magnetic resonance imaging (MRI), and tumor markers [21]. Ultrasound is the imaging method of choice for surveillance and an early HCC diagnosis, because it can detect tumors less than 1 cm in size. According to AASLD guidelines [22], a lesion less than 1 cm on ultrasound should be monitored with ultrasound at intervals of 3 to 6 months. Tumors bigger than 1 cm found by ultrasound screening should initiate recall procedures for the diagnosis of HCC and further undergo multiphase CT or MRI scan. For multiphase CT and MRI, key imaging features include size ≥1 cm, arterial phase hyperenhancement, and, depending on exact size, a combination of delayed venous phase washout, threshold growth, and capsule appearance. Liver biopsy should be considered when the lesion has atypical imaging features. Other possibilities include biomarkers such as embryonic antigen, protein antigen such as α-fetoprotein (AFP), enzymes and isoenzymes, cytokines, and genetic biomarkers. The Barcelona Clinic Liver Cancer (BCLC) classification (Figure 1) is the most widely accepted staging system; it is the only one that links the liver function, tumor stage, cancer-related symptoms and clinical performance status to an evidence-based treatment algorithm [22].

1.1.3.3 Treatments, the treatment of HCC includes curative therapies (including liver resection [LR], orthotopic liver transplantation [OLT] and ablation) and palliative therapies (including transarterial chemoembolization [TACE], transarterial radioembolization [TARE], stereotactic body radiation therapy [SBRT] and systemic therapy) (Figure 1).

In general, surgical resection, liver transplantation or ablation are the first choices for patients with early-stage HCC. According to the EMSO guidelines [23], Child-Pugh A patients without portal hypertension are considered as good candidates for LR. Carefully selected patients with Child-Pugh B and/or portal hypertension may be candidates for minor LR. LR in cirrhosis should preferably be carried out as laparoscopic resection. OLT should follow Milan criteria (one lesion < 5 cm; alternatively, up to three lesions, each < 3 cm; no extrahepatic manifestations; no evidence of macrovascular invasion). Thermal ablation by means of radiofrequency ablation (RFA) or microwave ablation (MWA) may be recommended as first-line treatment in very early stage disease. SBRT is an alternative option for thermal ablation, while prospective comparative randomized studies are needed. TACE/TARE is the standard of care for patients with intermediate stage HCC who are not eligible for curative treatments.

Systemic therapy for HCC changed drastically after the introduction of sorafenib, an oral multi-tyrosine protein kinases inhibitor, in 2007. Sorafenib is the first drug to demonstrate a survival benefit in advanced HCC patients with an improved mean overall survival (OS) from 7.9 to 10.7 months [24]. Sorafenib is recommended as the standard first-line systemic therapy for HCC and the treatment should be maintained at least until radiographic progression. Recently, lenvatinib, an oral multi-kinase inhibitor that targets vascular endothelial growth

factor receptor (VEGFR1-3); fibroblast growth factor receptor (FGFR1-4); platelet-derived growth factor receptor α (PDFGRα), RET and KIT [25], has been shown to be non-inferior to sorafenib in first line therapy. Regorafenib is an oral multi-kinase inhibitor that inhibits the activity of protein kinases involved in angiogenesis, oncogenesis and the tumour microenvironment [26]. Regorafenib showed survival benefits in patients with HCC who tolerated and progressed on sorafenib and improved the median OS from 7.8 months on placebo to 10.6 months. Thus, regorafenib have been approved by FDA and EMA as second-line options in patients with HCC who have been previously treated with sorafenib. Another category of agents that are attracting increasing interest are immune checkpoint inhibitors such as anti-PD-1/PD-L1 or CTLA-4 antibodies. Nivolumab, which targets PD-1, has been tested in several clinical trials and reported promising results in advanced HCC patients. Nivolumab's interference with the PD-1 receptor restores T-cell–mediated anti-tumour activity. The FDA has granted nivolumab conditional approval in second-line therapy for advanced HCC. And cabozantinib (a MET, VEGFR2 and RET inhibitor), pembrolizumab (anti-PD-1 antibody) etc. are also showing promising results in randomised clinical trials. These new drugs have shown a relevant improvement in survival and delay of tumor progression (Figure 1). Although multiple treatment options with molecular targeted agents and immune check-point inhibitors will benefit a wide range of HCC patients, adequate drug selection and clinical translation of genomic and tumor biological studies are still challenging for overcoming this fatal disease.

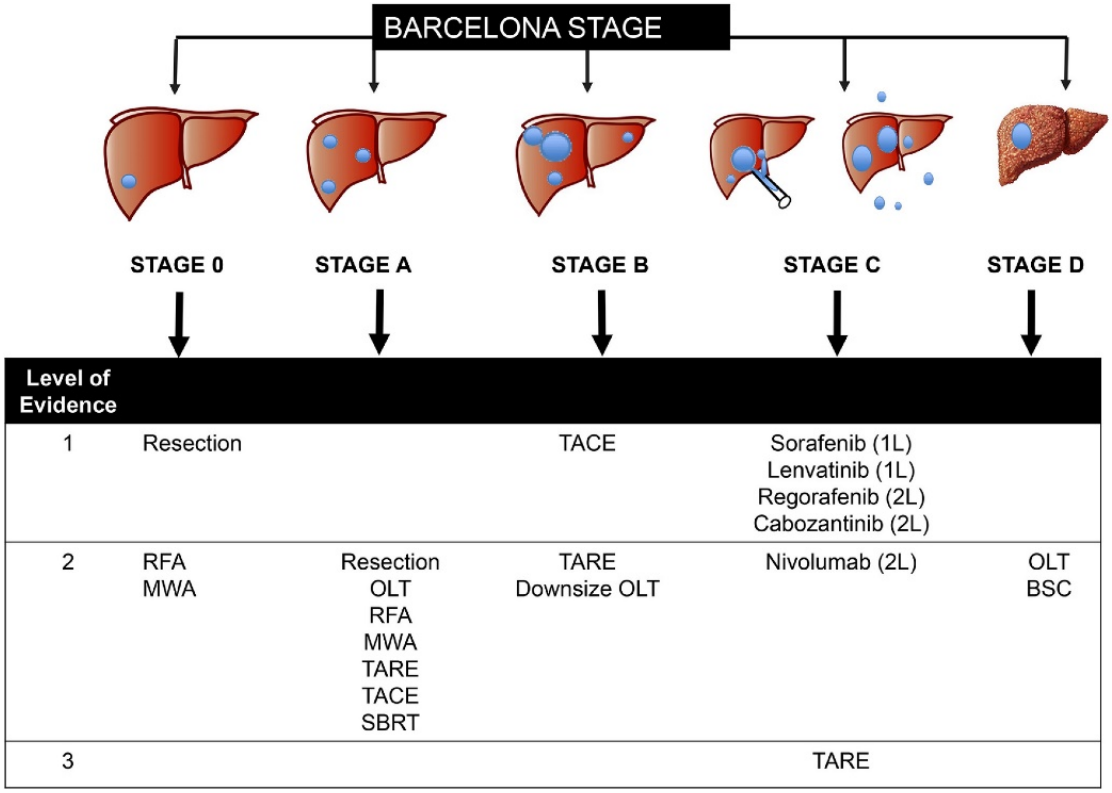

Level of Evidence					
1	Resection		TACE	Sorafenib (1L) Lenvatinib (1L) Regorafenib (2L) Cabozantinib (2L)	
2	RFA MWA	Resection OLT RFA MWA TARE TACE SBRT	TARE Downsize OLT	Nivolumab (2L)	OLT BSC
3				TARE	

Figure 1. Treatment recommendations according to BCLC Stage. Abbreviations: MWA, microwave ablation; BSC, best supportive care; 1L, first-line therapy; 2L, second-line therapy. [22]

1.1.4 Pathogenesis of HCC

Our understanding of the molecular pathogenesis of HCC has improved significantly in the last decade. Research have identified multiple key mutations and pathway alterations that occur during HCC carcinogenesis (Figure 2).

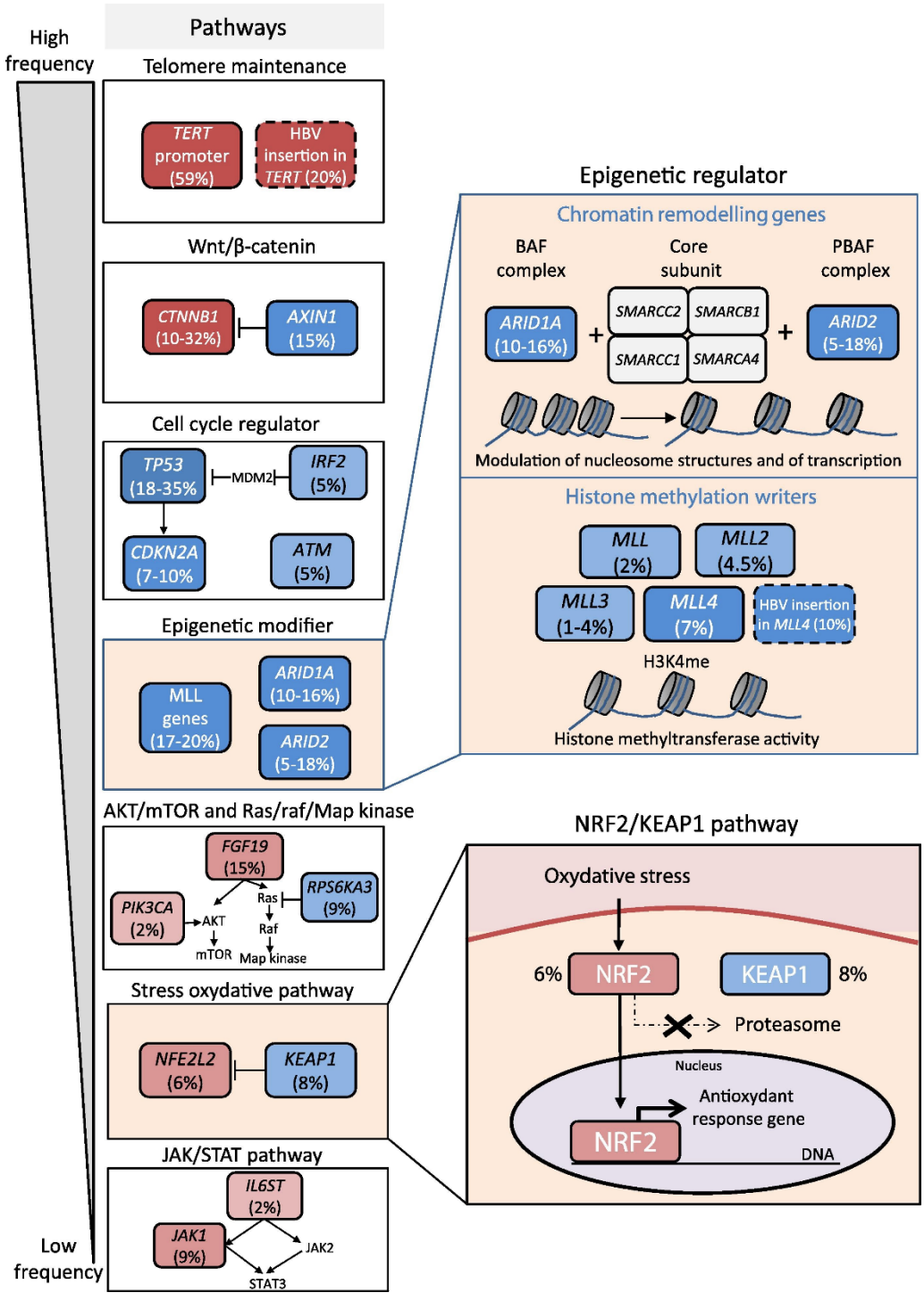

Figure 2. Major pathways altered in hepatocellular carcinoma. Signaling pathways recurrently mutated in HCC are shown in the right panel. Oncogenes are indicated in red and tumor-suppressor genes in blue with percentages of alterations. [27]

Angiogenesis and Growth factors

HCC is a highly angiogenic cancer characterized by an excess of angiogenic factors produced by tumor cells, vascular endothelial cells, immune cells, and surrounding tumor microenvironment [28]. Several growth factors are attributed to the angiogenesis, cell proliferation, and metastatic activity. Vascular endothelial growth factor (VEGF), platelet-derived growth factor (PDGF), epidermal growth factor (EGF), fibroblast growth factor (FGF) and insulin-like growth factor (IGF) are elevated in HCC patients [29]. Treatment for HCC have been associated with targeting these growth factors [29, 30].

Genetics and Signaling pathways

High-throughput genomic profiling technologies have identified an accurate landscape of genetic alterations in HCC. The most frequent mutations affect TERT promoter (60%–70%), associated with an increased telomerase expression [31]. TP53 (25%–50%) and CTNNB1 (25%–30%) are the next most prevalent mutations in HCC, however, untargetable [31]. In addition to these genetic modifications, signaling pathways were also associated with the carcinogenesis of HCC, including, the Wnt/β-catenin pathway, Ras/Raf/MEK/Erk pathway and the PI3K/Akt/mTOR pathway [31, 32].

1.2 Rb/E2F Pathway

RB1 gene was the first gene identified as a potential tumor suppressor gene due to its mutation in retinoblastoma [33-36]. The product of this gene – Rb – is considered as a multifunctional protein. Numerous studies have identified Rb as a central player in cell cycle regulation [37-39] and elucidated its interaction with E2F transcription factors, a family of cell-cycle regulated transcription factors that stimulate proliferation [40-42]. Inactivation of the Rb protein is one of the

most fundamental events in cancer. Also the Rb tumor suppressor pathway is frequently disrupted in HCC [31, 43]. Moreover, several studies have disclosed additional tumor-suppressor functions of Rb, including alternative roles in the cell cycle regulation, maintenance of genomic stability and apoptosis [44, 45].

The mammalian cell cycle is divided into four phases that include gap phase G1, DNA synthesis (S), mitosis (M) and gap phase G2. The proliferation of mammalian cells is normally stimulated by extracellular signal molecules which communicate with cell surface receptors and trigger a program of gene expression and protein regulation [46]. Expression of these groups of cell cycle dependent genes is rigorously modulated by the Rb/E2F pathway.

Rb protein exists in three differentially phosphorylated forms in eukaryotic cells: un-phosphorylated, mono (hypo)-phosphorylated and multi (hyper)-phosphorylated. The first two forms of Rb bind to E2F transcription factors [47]. Initially Rb is un-phosphorylated in quiescent cells; but when cells are stimulated by proliferation signal to enter the cell cycle, Rb becomes mono-phosphorylated by cyclin D–CDK4/6 complexes [47]. In late G1, when cells pass the restriction checkpoint, cyclin E–CDK2 complexes multi-phosphorylate the mono-phosphorylated Rb, which leads to inactivation of Rb and its release from E2F. When a quiescent cell is triggered to enter the cell cycle, it starts expressing cyclin D which assembles into complexes with CDK4/6, and is capable to mono-phosphorylate the Rb pocket proteins [47]; at this period, CDK2 complexes are inactivated by the CDK inhibitor p27. In late G1 phase, Rb becomes multi-phosphorylated by cyclin E–CDK2 complexes, leading to its dissociation from E2F1–3 transcription factors [47]; this event is pivotal for cells to pass the restriction point [48] and facilitating S phase entry. The whole

process is simplified and depicted in Figure 3. When cells proceed through S phase, cyclin A-CDK2 complexes become active, and phosphorylate E2F transcription factors, which terminates the transcription of E2F responsive genes. The key role of Rb/E2F pathway in regulating cell cycle progression and controlling proliferation offers tremendous potential for the development of therapeutics.

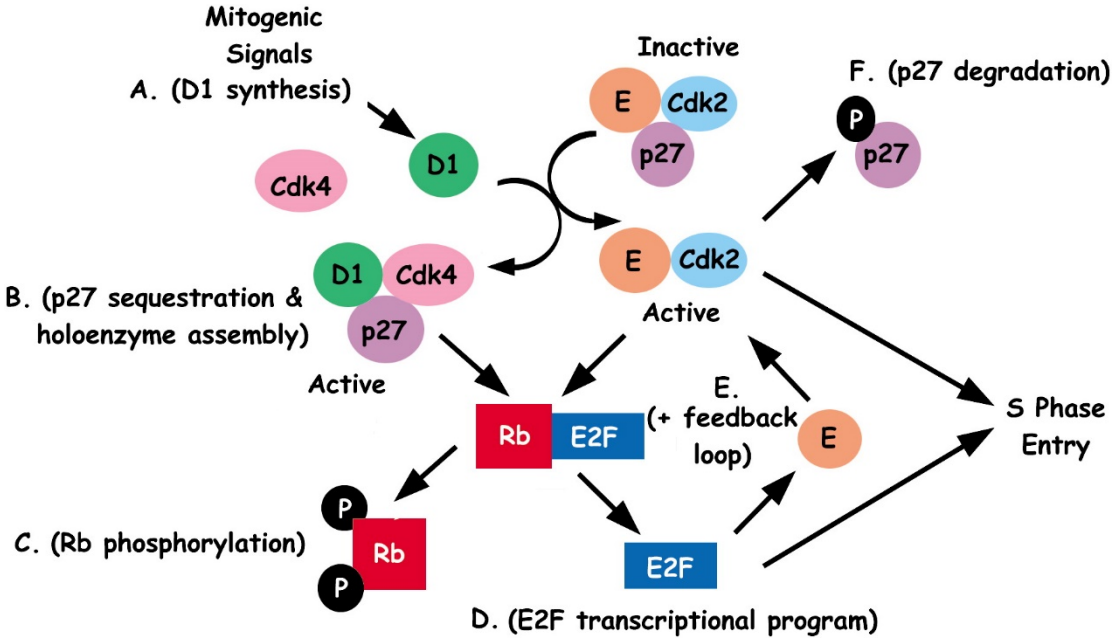

Figure 3. G1 phase regulatory cascade Cyclin D1 synthesis (step A) and assembly (step B) in response to mitogenic signals sequesters Cip/Kip proteins (p27Kip1 is shown) and relieves cyclin E-Cdk2 from their constraint. Both G1 cyclin-dependent kinases then collaborate to sequentially phosphorylate RB family proteins (only RB is shown) (step C). This frees E2Fs from inhibition and leads to the activation of genes required for S phase entry (step D). Among the known E2F target genes is *cyclin E*, whose transcriptional upregulation provides positive feedback to drive cells into S phase (step E). One substrate of cyclin E-Cdk2 is p27Kip1, whose phosphorylation triggers its ubiquitination and degradation as cells enter S phase (step F). [49]

1.3 Akt/mTOR Pathway

The serine and threonine kinase Akt, also known as protein kinase B (PKB), was discovered in 1991 and has been the focus of tens of thousands of studies in diverse fields of biology and medicine [50-52]. There are three Akt isoforms conserved in mammalian genomes: Akt1 (PKB α), Akt2 (PKB β), and Akt3 (PKB γ). The PI3K/Akt/mTOR signaling cascade is another major signaling pathway implicated in HCC carcinogenesis and plays a central role in a driving tumor cell proliferation [43, 53]. This pathway is a prototypic survival pathway that is constitutively activated in many types of cancer and involved in a broad range of cellular processes including survival, proliferation, growth, metabolism, angiogenesis and metastasis [53-55]. Given the frequent hyperactivation or deregulation of Akt/mTOR pathway in HCC [55-57], several small molecule inhibitors targeting this pathway have been developed and are currently undergoing pre-clinical or clinical trials [43, 58].

Upstream Regulation of Akt

The canonical pathway causing Akt activation is initiated by the stimulation of receptor tyrosine kinases (RTK) or G protein-coupled receptors (GPCR) resulting in cytoplasmic membrane relocalization and activation of isoforms of the class I PI3K family (Figure 4). Pleckstrin homology (PH) domain is engaged in the recruitment of inactive Akt to membrane sites of $PI3,4P_2$ or PIP_3 accumulation. Activation of PI3K leads to the phosphorylation of two key residues on Akt1, Thr308 and Ser473 [59]. The phosphoinositide dependent protein kinase 1 (PDK1) was discovered to phosphorylate Akt1 at Thr308, which is requisite for Akt1 activity [60, 61]. The principal Akt Ser473 kinase is the mammalian target of rapamycin complex 2 (mTORC2) [62]. Whereas Akt lacking Ser473 phosphorylation has activity, it is notably diminished, and

phosphorylation of Ser473 stabilizes Thr308 phosphorylation and the activation state of Akt [59, 63]. Phosphorylation of both residues is vital for maximal activation of the kinase. Lipid phosphatases such as PTEN and INPP4B, and protein phosphatases such as PP2A and PHLPP directly inactivate Akt which contributes to signal termination.

Generally, Akt activation promotes cell survival, proliferation, growth, metabolism, angiogenesis and metastasis through its extensive downstream targets. Among these, GSK3, FoxO and mTORC1 are the three best-established downstream targets of Akt and key signaling nodes that integrate Akt with alternative cellular regulatory circuits (Figure 4).

Glycogen Synthase Kinase 3

The multi-functional protein kinase: glycogen synthase kinase 3 (GSK3) was the first reported Akt substrate [64]. GSK3 is inherently activated in the absence of upstream signals and directly regulates a large set of functionally diverse downstream targets, most of which are inhibited or degraded upon GSK3-mediated phosphorylation including the prosurvival BCL-2 family member MCL-1 [65-67] and the transcription factor c-Myc [68-70]. Akt exerts an inhibitory effect on both GSK3α and GSK3β by serine phosphorylation. Therefore, growth factor signaling through Akt positively regulates and stabilizes these targets through the inhibition of GSK3.

Forkhead Box O Family Transcription Factors

The Forkhead Box O (FoxO) family transcription factors, comprised of FoxO1, 3, 4 and 6, control a series of genes involved in adaptation to fasting and low insulin and response to IGF1 signaling [71, 72]. Activation of PI3K-Akt signaling results in prompt translocation of FoxO proteins from the nucleus to cytoplasm

and attenuation of their transcriptional activities [73, 74]. Therefore Akt signaling suppresses the expression of FoxO target genes involved in the cell cycle arrest (e.g., p21 and p27), induction of apoptosis (e.g., BIM and PUMA), catabolism and growth inhibition (e.g., Sestrin3, MAP1LC3B, and BNIP3), and tissue-specific metabolic changes (e.g., PEPCK and G6PC) [71, 72].

Tuberous Sclerosis Complex 2 and mTORC1

PI3K/Akt signaling pathway is an evolutionarily conserved pro-survival pathway. This regulation is predominantly mediated through the protein kinase complex mTORC1, which promotes the biosynthetic processes underlying cell growth [75]. Akt activates mTORC1 primarily through the phosphorylation and inhibition of tuberous sclerosis complex 2 (TSC2) [76-78]. TSC2 is a GTPase-activating protein (GAP) specific for the Ras-related GTPase, Rheb, which is an essential activator of mTORC1. The TSC complex is a potent inhibitor of mTORC1. The Akt-mediated phosphorylation of TSC2 immediately releases of the TSC complex from Rheb, thereby relieves its inhibition and activates mTORC1. Subsequently, mTORC1 phosphorylates and activates the ribosomal protein S6 kinase (S6K1 and S6K2), whose substrate was rpS6 (ribosomal protein S6), a component of the 40S ribosome in eukaryotic cells, correlating with an increase in translation of mRNA transcripts. It is also worth noting that Akt has been suggested to directly phosphorylate mTOR on Ser2448 [79, 80].

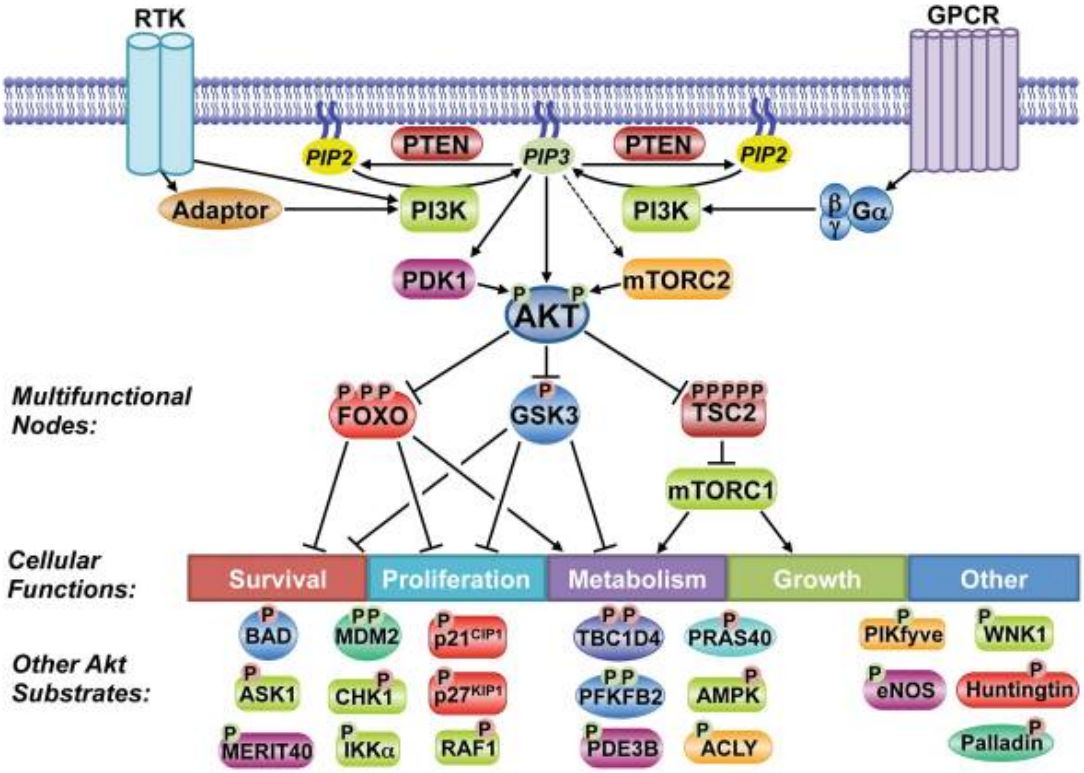

Figure 4. Substrates and functions of the Akt signaling network. Akt phosphorylates downstream substrates involved in the regulation of diverse cellular functions, including multifunctional substrates. A partial list of known substrates is shown. P indicates phosphorylation, with red and green denoting inhibitory and activating regulation, respectively. [53]

1.4 Haprolid

Myxobacteria are well-established sources for novel natural products which exhibit a broad spectrum of intriguing bioactivities. Haprolid (Figure 5) was isolated from the myxobacterium *Byssovorax cruenta* strain Har1 at the Helmholtz Centre for Infection Research GmbH (HZI) already in 2000 [81]. Haprolid compound is a polyketide-peptide hybrid which presents an unprecedented macrolactone comprising four modified amino acids and a polyketide fragment. This compound was obtained as white powder and was assigned as a molecular formula of $C_{38}H_{58}N_4O_7$ on the basis of high-resolution electrospray ionisation mass spectrometry (HR-ESI-MS) data. Haprolid has been firstly identified as a novel, potent HCV inhibitor which affects assembly

and release of HCV particles as well as HCV replication. However, this compound was determined to influence the host cell rather than the virus itself. Furthermore, Haprolid has been tested on a panel of human cancer cell lines and demonstrated intriguing and selective cytotoxic activity.

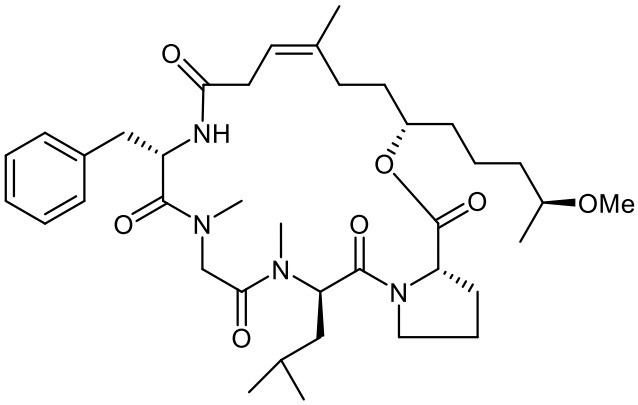

Figure 5. Chemical structure of Haprolid.

The compound was highly active (IC50 values in low to middle nanomolar range) on the cervix carcinoma cells lines Hep2 and KB-3.1, and leukemia cell lines THP-1 and HL-60. The IC50 values on HCC cell line Huh7.5 and osteosarcoma cell line U-2 OS were in the high nanomolar range. In contrast, Haprolid is not sensitive on A-549 lung carcinoma cells and SK-OV-3 ovarian adenocarcinoma cells. The reason for the selective cytotoxicity is currently unknown as well as the molecular target of this compound. Future studies are unmet needed to address the intriguing question of the mode of action of the Haprolid class of natural metabolites. In summary, the remarkable biological activities associated with its short and efficient synthesis procedure (12 steps in the longest linear sequence) provide the background for potential biological application of this compound. Based on these studies, we set out to identify the antitumor effect of Haprolid on HCC.

2. Materials and Methods

2.1 Materials

2.1.1 Expendable items

12-well plate	Falcon, Wiesbaden
15 ml culture tube	Falcon, Wiesbaden
24-well plate	Falcon, Wiesbaden
50 ml culture tube	Falcon, Wiesbaden
6-well plate	Falcon, Wiesbaden
96-well plate	Falcon, Wiesbaden
Cell culture dishes 1000mm	Sarstedt, Nümbrecht
Cell culture dishes 60mm	Sarstedt, Nümbrecht
Centrifuge tubes	Eppendorf, Hamburg
Cover slip	Menzel-Glaeser, Darmstadt
Filter tips 0,1-10 ul	Sarstedt, Nümbrecht
Filter tips 1000 ul	nerbe plus, Winsen
Filter tips 20 ul	Sarstedt, Nümbrecht
Filter tips 200 ul	nerbe plus, Winsen
Freezing tube	Thermo Fisher Scientific, Darmstadt
Hyperfilm TM ECL	GE Healthcare, Darmstadt
Microscope slides	R. Langenbrinck GmbH, Emmendingen
Tips 20-200 ul	Sarstedt, Nümbrecht
Transfer membrane	Immobilon, Darmstadt
Whatman paper	GE Healthcare, Darmstadt

2.1.2 Equipments

Centrifuge	Thermo Scientific, Darmstadt
Centrifuge	Hettich, Tuttlingen
Clean bench	Heraeus, Hanau
Clean bench	ENVAIR, Emmendingen
Fluorescence microscope	Olympus, München
Gel electrophoresis systems	Bio-RAD, München
Heater	Heidolph Instruments, Schwabach
Incubator	Thermo Scientific, Darmstadt
Magnetic stirrers	neoLab Migge, Heidelberg
Mixer 5432	Eppendorf, Hamburg
Multipette® plus	Eppendorf, Hamburg
Pipetman	Gilson, Limburg-Offheim
Pipett	Eppendorf, Hamburg
Vortex-Genie	Scientific Industries, Darmstadt
Water bath	GFL, Burgwedel

2.1.3 Software

FlowJo Version 10 (FlowJo, LLC, Ashland)

ImageJ 1.47 (Wayne Rasband, National Institutes of Health)

GraphPad Prism 8 (GraphPad Software, San Diego)

2.1.4 Chemicals

ABC-peroxidase kits		Vector, Eching
Acrylamid-solution (30%)	37,5:1	Carl Roth, Karlsruhe
Agar		BD Biosciences, Heidelberg

Albumin FrAktion V	Carl Roth, Karlsruhe
Ammonium persulfate	Sigma-Aldrich, Schnelldorf
Ammonium sulfate	AppliChem, Darmstadt
Annexin V apoptosis kit	BD Biosciences, Heidelberg
Boric acid	AppliChem, Darmstadt
Calcium chlorid	AppliChem, Darmstadt
Caspase inhibitor I	Biochrom, Berlin
Cesium chloride 99%	AppliChem, Darmstadt
Crystal violet	Sigma-Aldrich, Schnelldorf
DAB substrate Kit	Vector, Eching
DMF (Dimethylformamide)	Sigma-Aldrich, Schnelldorf
DMSO	AppliChem, Darmstadt
EDTA	AppliChem, Darmstadt
EGTA	AppliChem, Darmstadt
Ethanol	AppliChem, Darmstadt
FBS	Biochrom, Berlin
Gelatine	Sigma-Aldrich, Schnelldorf
Glucose	Sigma-Aldrich, Schnelldorf
Glycine	AppliChem, Darmstadt
Haprolid	Leibniz Universität, Hannover
HEPS	AppliChem, Darmstadt
Histol	Carl Roth, Karlsruhe
Hydrogen peroxide solution	Merck, Darmstadt
Magnesium chloride	AppliChem, Darmstadt
Methanol	AppliChem, Darmstadt
MG132	Sigma-Aldrich, Schnelldorf
Mounting medium	Vector, Eching

Nonfat dried milk powder	AppliChem, Darmstadt
Nonidet® P40	AppliChem, Darmstadt
Paraformaldehyde	Sigma-Aldrich, Schnelldorf
Penicillin-streptomycin solution	Lonza, Belgium
Ponceau S solution	Roth, Karlsruhe
Potassium chlorid	AppliChem, Darmstadt
Potassium dihydrogen phosphate	Merck, Darmstadt
Propidium iodide	Sigma-Aldrich, Schnelldorf
SDS	AppliChem, Darmstadt
Senescence Kit	CST, Frankfurt
Sodium azide	Sigma-Aldrich, Schnelldorf
Sodium chloride	VWR, Darmstadt
Sodium dihydrogen phosphate	Merck, Darmstadt
Sodium fluoride	AppliChem, Darmstadt
Sodium hydroxide	Merck, Darmstadt
Sodium pyruvate	AppliChem, Darmstadt
ß-Mercaptoethanol	AppliChem, Darmstadt
TEMED	AppliChem, Darmstadt
Toluidine blue	Sigma-Aldrich, Schnelldorf
Tris base	Sigma-Aldrich, Schnelldorf
Triton X 100	AppliChem, Darmstadt
Trypsin/EDTA solution	Lonza, Belgium
Tween-20	AppliChem, Darmstadt
Urea	Merck, Berlin
WST-1	Roche, Mannheim

2.1.5 Buffers and Solutions

RIPA-buffer

	Stock	Final	for 500 ml
NP40	10%	1%	50 ml
DOC	10%	0.5%	25 ml
SDS	10%	0.1%	5 ml
Tris pH 8.0	1 M	50 mM	25 ml
NaCl	5 M	80 mM	10 ml
NaF	0.5 M	50 mM	25 ml
Na4P2O7	1 M	20 mM	4.26 ml
EDTA	0.5 M	1 mM	1 ml
EGTA	0.5 M	1 mM	1 ml
H2O			358 ml
Total			500 ml

Separating gel

	7.5%	10%	12%	14%	15%
Acrylamide	2.5 ml	3.3 ml	4.0 ml	4.7 ml	4.95 ml
Tris pH 8.8	2.5 ml	2.5 ml	2.5 ml	2.5 ml	2.5 ml
H2O	4.85 ml	4.1 ml	3.4 ml	2.7 ml	2.45 ml
10 % SDS	100 ul	100 ul	100 ul	100 ul	100 ul
TEMED	15 ul	15 ul	15 ul	15 ul	15 ul
10 % APS	105 ul	105 ul	105 ul	105 ul	105 ul

Stacking gel

Acrylamide	30%	1.13 ml
Tris 6.8 pH	0.5M	1.75 ml
ddH2O		3.92 ml
SDS	10%	70 ul
TEMED		7 ul
APS	10%	70 ul

Western SDS running buffer (10x)

Tris	151 g
SDS	50 g
Glycine	720 g

with H_2O to 5L

Western transfer buffer (10x)

Tris	151 g
Glycine	720 g

with H_2O to 5L

TBST buffer (10x)

Tris	60.57 g
NaCl	438.3 g
Tween 20	25 ml

with millipore H_2O to 5L

2.1.6 Antibodies

Primary antibody

Akt(pan)	Cell signaling	4685	60kDa

CDK2	Cell signaling	2546	33kDa
cyclin A	Santa cruz	sc-751	54kDa
cyclin B1	Santa cruz	sc-245	60kDa
E2F-1	Cell signaling	3742	70kDa
E-Cadherin	Cell signaling	3195	135kDa
Ki-67	Leica	NCL-L-Ki67-MM1	359kDa
mTOR	Cell signaling	2983	289kDa
N-Cadherin	Cell signaling	13116	140kDa
p- H3(Ser10)	Abcam	ab5176	17kDa
p- H3(Ser10)	Cell signaling	3377	17kDa
p21	Santa cruz	sc-397	21kDa
p27 Kip1	Cell signaling	2552	27kDa
p-Akt(Ser473)	Cell signaling	9271	60kDa
PARP	Cell signaling	9542	89,116kDa
p-Erk1/2	Cell signaling	4370	42,44kDa
p-mTOR(Ser2448)	Cell signaling	2971	289kDa
p-mTOR(Ser2481)	Cell signaling	2974	289kDa
p-p70S6K(Thr389)	Cell signaling	9205	70,85kDa
p-Rb(Ser807/811)	Cell signaling	9308	110kDa
p-S6(Ser240/244)	Cell signaling	5364	32kDa
Rb	Cell signaling	9313	110kDa
S6	Cell signaling	2217	32kDa
Snail	Cell signaling	3879	29kDa
Vimentin	Santa cruz	sc-7557	57kDa
β-actin	Santa cruz	sc-47778	43kDa

Secondary antibodies

Anti-mouse IgG, Horseradish Peroxidase linked antibody (from sheep)	1:10000	Amersham, NA931
Anti-Rabbit IgG, Horseradish Peroxidase linked antibody (from donkey)	1:10000	Amersham, NA934

2.2 Methods

2.2.1 Cell Culture

All aseptic operations were performed under a laminar flow hood and all items used were disinfected properly. Three human HCC cell lines: Hep3B, Huh-7 and HepG2 were used in this experiment. Huh-7 cells were provided by the laboratory of Lars Zender (University Hospital Tübingen, Germany). HepG2 cells were provided by the laboratory of Michael Bitzer (University Hospital Tübingen, Germany). Hep3B was purchased from Leibniz institute DSMZ-German collection of microorganisms and cell cultures. The cell lines were maintained at 37°C under a 5% CO_2 environment in Dulbecco's Modified Eagle Medium (DMEM) enriched with 10% Fetal Bovine Serum (FBS) and antibiotics of penicillin/streptomycin (50 units/ml). The cells were passaged every 3 to 4 days.

2.2.2 Drug Preparation and *in vitro* Treatment

Haprolid was supplied by the department microbial drugs, HZI, Braunschweig, Germany. The compound was isolated from the culture broth of *Byssovorax cruenta* using the chromatographic procedure described by Steinmetz et al. [81]. The drug was prepared as a 10 mg/ml stock in Dimethyl sulfoxide (DMSO). Haprolid was divided in aliquots, stored at 4°C and used for *in vitro* and *in vivo*

experiments. Cells were treated with DMSO as a control or Haprolid of indicated concentrations and analyzed after certain time points.

2.2.3 Determination of Cell Viability and Proliferation using WST-1 Assay

The cell viability was determined by the WST-1 assay. Living cells with a functional mitochondrial dehydrogenase will catalyze the red WST-1 (water soluble tetrazolium salts) to orange formazan dye. Quantification of the formazan dye by measuring the absorbance at certain wavelength for our cases 450 nm directly correlates to the number of metabolically active cells in the culture. A total $2x10^3$ cells with 200 µl complete media were seeded per well into 96-well plates and PBS was pipetted into the surrounding wells in order to keep the media from drying. Following the indicated treatment HCC cells were further incubated for additional time points of 24 hrs, 48 hrs, 72 hrs and 96 hrs respectively. Then 20 µl of WST-1 reagent was added per well and incubated for another 2 hours at 37°C before reading. The plates were read at a wavelength of 450 nm with a reference wavelength of 690 nm according to the manufacturer's datasheet using a Microplate Reader Synergy™ HT.

2.2.4 Apoptosis Assays

Apoptosis is a form of programmed cell death (PDS) that may occur during many physiologic and pathologic processes in multicellular organisms. The apoptotic program is characterized by certain morphologic features, chromatin condensation, chromosomal DNA fragmentation and global mRNA decay. Loss of plasma membrane asymmetry and cell attachment is one of the earliest features of PDS. In apoptotic cells, the membrane phospholipid phosphatidylserine (PS) is translocated from the inner to the outer leaflet of cell membrane. Annexin V is a 35-36 kDa Ca^{2+} dependent phospholipid-binding

protein which has a high affinity for PS. Since externalization of PS occurs in the earlier stages of apoptosis, Annexin V staining can identify apoptosis at an earlier stage compared with the other assays based on nuclear changes such as DNA fragmentation. Viable cells with intact membranes exclude propidium iodide (PI), whereas the membranes of dead or damaged cells are permeable to PI. Therefore, staining with Annexin V is typically used in combination with a vital dye such as PI to allow the investigator to identify early apoptotic cells. Thus living cells are Annexin V and PI negative. Early apoptotic cells are Annexin V positive and PI negative. Late apoptotic cells or dead cells are both Annexin V and PI positive. The quantitative measurement of the percentage of apoptotic cells can be performed in the whole cell population.

Cells were seeded in 6-well plates at a density of $2x10^5$ cells per well and were incubated overnight at 37°C. These cells were further treated with Haprolid (0.06, 0.6 and 6 µg/ml) or DMSO. After 48 hrs and 96 hrs incubation, the supernatant (floating apoptotic cells) was collected and the adherent cells were trypsinized and then collected to the same tube. The tubes were centrifuged for 5 mins at 1000 rpm. The supernatant was discarded, the cell pellet was suspended with 1 ml 1 X Binding Buffer at a concentration of approximately 1×10^6 cells/ml on ice. The untreated control group was divided into three tubes (Annexin V signal staining control, PI signal staining control and unstained control). Transfer 100 µl of the solution (1×10^5 cells) to a 5 ml FACS tube. 3 µl Annexin V was added to the tube and incubated in dark on ice for 7-8 mins then 3 µl PI was added and incubated in dark for another 7-8 mins. Afterwards 400 µl of 1 X Binding Buffer was added to each tube. The prepared sample should be analyzed by flow cytometry within one hour. The signal was detected using FACS Canto II and analyzed using FlowJo Version 10 software.

2.2.5 Wound Healing Assay

Metastasis is one of the hallmarks of cancer, which distinguishes malignant tumors from benign. Migration and invasion are key steps to initiate cancer metastasis. The *in vitro* scratch assay is an easy, low-cost and well-developed method to measure cell migration.

HCC cells were seeded in a 6-well plate and left to reach about 80% confluence. Initially, cells were starved for 24 hrs in media containing 2% FBS in order to minimize the interference of cell proliferation. Then HCC cell lines were further incubated for 48 hrs in the starvation media containing either the controls (DMSO) or Haprolid. Afterwards a scratch was done using a 200 µl pipette tip under an angle of around 30 degrees. Then cells were washed with pre-warmed PBS and snapshot pictures were taken using a regular inverted microscope. Cells were incubated for an additional 24 hrs after which photographs were taken for the wounded area. The migration index was calculated using the following formula:

$$Migration\ Index = \frac{Width\ of\ the\ wound_{0h} - Width\ of\ the\ wound_{24h}}{Width\ of\ the\ wound_{0h}} \times 100$$

2.2.6 Invasion Assay

The Corning® BioCoat™ Matrigel® invasion chamber is a well-established system to study cell invasion *in vitro*. The inserted chamber contains an 8 µm size pore PET membrane with a thin layer of matrigel basement membrane matrix. Only invasive cells which are driven by the chemoattractant are able to invade through the extracellular matrix-like environment and the membrane pores to reach the other side of the membrane.

The invasion chamber (stored at -20°C) was warmed at room temperature and rehydrated with serum-free media for 2 hours in 37°C incubator according to the datasheet. Subsequently, the rehydrated media were removed and a number of $2x10^4$ cells were plated in the upper chamber filter with 0.5 ml serum free media. Simultaneously the cells were treated with Haprolid (0.06, 0.6 and 6 µg/ml) or DMSO. These upper chambers were carefully placed into the 24-well plate containing media supplemented with 20% FBS as a chemoattractant. After 48 hrs incubation at 37°C, 5% CO_2 atmosphere the cells on the upper surface of the membrane were mechanically removed using a cotton swab. The invading cells were fixed 2 mins in 100% ice-cold methanol and stained 2 mins with 1% toluidine blue in 1% borax. After staining the membrane was removed from the insert and placed on a microscope slide. Cells were then counted under the microscope at 200 X magnifications. The following calculation of the invasion index was done according to the manufacturer's protocol:

$$Invasion\ Index = \frac{\%\ Invasion\ Test\ Cell}{\%\ Invasion\ Control\ Cell}$$

2.2.7 Western Blotting

Protein Extraction

HCC cells in 100 mm culture dish treated with 16 ml DMSO or Haprolid (0.06, 0.6 and 6 µg/ml) for indicated time points were collected and transferred to 15 ml Falcon tubes and centrifuged for 5 mins at 1000 rpm. The supernatant was discarded, the cell pellet was resuspended and washed with cold PBS and centrifuged again. The supernatant was discarded and the cell pellets were digested in RIPA lysis buffer (ca. $5x10^6$ cells/200 µl) supplemented by protease

and phosphatase inhibitors for 30 mins on ice. Next, sonification was made on ice (20W, 15 seconds per cell pellet) for disturbance of the intact cell membrane. The suspensions were centrifuged for 20 mins at 13300 rpm at 4°C. Then the supernatant was carefully transferred into Eppendorf tubes and the protein concentration was further determined.

Protein Quantification

The protein quantification was conducted according to the manufacturer's instructions with the Bio-Rad DC protein assay. The assay is based on the reaction of protein with an alkaline copper tartrate solution and Folin reagent which leads to characteristic blue color development with maximum absorbance at 750 nm. The absorbance was measured with the Microplate Reader Synergy™ HT. The value of protein concentration was averaged from triplicated wells and calculated according to the BSA standard curve. Then different tubes were normalized by adding lysis buffer and protein loading dye.

Electrophoresis

The glasses plates were carefully cleaned with 70% ethanol and dried. The separating gel was poured between two glasses plates and then sealed with 100% ethanol. After 30 mins, the ethanol was removed. The stacking gel was poured on top of the separating gel. The gel was placed into the electrophoresis chamber and filled with 1×SDS running buffer. Before the samples were loaded, they were boiled for 5 mins at 95°C and then mixed well. Page ruler plus pre-stained protein ladder was used as protein markers. Electrophoretic separation was carried out at 60-65 V until the separating gel was reached, then the voltage was increased to 120-125 V.

Protein Transfer to PVDF Membrane

The PVDF membrane was briefly incubated in 100% methanol around 10 s, and then put in 1x western transfer buffer. When assembling the blotting-sandwiches (from cathode to anode: holder / sponge / Whatman paper / gel / PVDF membrane / Whatman paper / sponge / holder) bubbles were removed thoroughly. The protein transfer was performed at 4°C, 0.35 mA and 90 V for 1 hr. Subsequently, the PVDF membrane was washed 10 mins and shifted to the blocking solution (5% non-fat milk or 5% BSA in TBST) for 1-3 hrs and then the membrane was washed with 1xTBST buffer 3 times for 10 mins on the shaker.

Antibody Detection

These membranes were further probed with primary antibodies at 4°C overnight. The next day the primary antibodies were recollected and the membrane was washed 3 times for 10 mins with 1xTBST. And then the membrane was incubated for 1 hr at room temperature with the secondary antibody. After another three times wash with 1xTBST the signal was detected by Amersham Hyperfilm^{TM} ECL. The exposure time varies from 10 s to 20 mins for relative antibodies.

2.2.8 Cell Cycle Analysis

The DNA of mammalian cells can be stained by a variety of DNA binding dyes. The binding of these dyes is in proportion to the amount of DNA present in the cell, thus the cells in G2 phase will be approximately twice as bright as cells in G1 phase. In this way the cell cycle distribution can be readily profiled using flow cytometry analysis.

To figure out the cell cycle distribution after Haprolid treatment, $2x10^5$ HCC cells were seeded in a 6-well plate and treated as indicated. At certain time points, cells were harvested in an appropriate manner and washed with PBS and then fixed with 70% ice cold ethanol in -20°C. Alcohol-fixed cells are stable for several weeks at -20°C. These cells were further centrifuged and washed with cold PBS. Then cells were stained with 10 µg/ml of PI and 50 µg/ml ribonuclease in PBS and incubated for at least 45 mins at room temperature in dark. The signal was detected using flow cytometer Canto II and analyzed using FlowJo Version 10 software.

2.2.9 Animal Experiment

Therapeutic studies *in vivo* were performed with NMRI-Foxn1^{nu} female mice. The animal without thymus is unable to produce T-cells, and is, therefore, immunodeficient. These mice were bought from Charles River Laboratories International (Sulzfeld, Germany). 8 mice were treated intraperitoneally with Haprolid (2 mg/kg body weight, on day 1 to day 3 each week), 6 mice were treated with vehicle (DMSO: Tween20: ddH_2O, 1: 1: 8). Treatment was started around 10 weeks of age and mice were sacrificed after 5 weeks of treatment. All treatment solutions were prepared freshly on the day of delivery. Health status of mice was monitored every day. Sizes of visible tumors were measured by caliper and organ tissues were harvested. Tumor volume was calculated using the following formula: Tumor volume V = [$(Width)^2$ × (Length) /2]. Tumor tissues were fixed in 4% formalin for histology.

Ethics Statement

Mice used in this study were maintained in the animal care of University Hospital Tübingen, Germany. All experimental protocols were reviewed and approved by institutional guidelines for animal care of University Hospital Tübingen (protocol Nr.: M7/17), and all studies were performed according to the methods approved in the protocol.

2.2.10 Immunohistochemistry (IHC)

IHC is a method for demonstrating the presence and location of proteins in tissue sections. In brief, the primary antibody is specific bound to the protein of interest. A biotinylated secondary antibody is then bound to the primary antibody. After antibody incubations, avidin-biotin complex (ABC) is used to amplify the signal. 3,3'-diaminobenzidine (DAB) served as a substrate of Horseradish peroxidase (HRP) to generate intensive and permanent brown color which makes the antigen visible.

Formalin-fixed, paraffin sections were kept in 55°C overnight to melt excess wax (unnecessary for small sections) and then deparaffinized in histol and rehydrated in ethanol (100%, 95%, 75% and 40% ethanol). Afterwards the sections were rinsed three times for 3-5 mins with PBS and then subjected to antigen retrieval by heating the slides in a pressure cooker with antigen unmasking solution. Bring 1.6 L unmasking solution to boil and then add the slides in a clean metallic slide holder and seal lid. Wait 15 to 20 mins till the pressure cooker reaches its certain pressure and then maintain for 1 min. Afterwards reduce the pressure immediately under running cold water and gently take out the slides. The specimens were rinsed twice 3-5 mins with PBS and were then incubated for 10 mins in 1% H_2O_2 to inactivate endogenous

peroxidase activity. The slides were further blocked 1 hr in blocking solution (5% normal goat serum in 0.3% Triton X-100) at room temperature to avoid non-specific binding. Hybridization with the primary antibody (1:100) was carried out overnight at 4°C. The next day, the primary antibody was rinsed by PBS and the slides were incubated with secondary antibody (1:200) for 1 hr. The manufacturer's protocols were used for ABC and DAB substrates. Then, the slides were counterstained with hematoxylin for 1 min and dehydrated in 40%, 75%, 95%, and 100% ethanol. Finally, the slides were cleared with histol and mounted with mounting medium. The histology was reviewed by professional pathologist. Images were taken by light microscope and positive cells were quantified using software Image J.

2.2.11 Statistical Analysis

All the experiments were repeated 2-3 times. The results were analyzed using software GraphPad prism version 8.0 and Image J 1.47. The tests include Student's t-test (paired and unpaired) and two-way ANNOVA analysis of variance. Differences were considered as statistically significant when the P-value was <0.05 (*), <0.01 (**), <0.001 (***), <0.0001 (****) or as not significant "ns".

3. Results

3.1 Haprolid treatment inhibits proliferation, migration and invasion of human HCC cell lines

In 2016, it was shown that Haprolid (Figure 5) has anti-tumor effects against various tumor cells [81]. However, data about HCC and Haprolid are limited. Therefore, we determined the cytotoxic effect of Haprolid on three human HCC cell lines (Hep 3B, Huh-7 and HepG2) by WST-1 assay. In addition, human fibroblasts, as non-cancer cells, were similarly tested to display differential cytotoxicity (Figure 6). The concentration for 50% of maximal inhibition of cell proliferation (IC50) for Hep3B, Huh-7 and HepG2 cells after 96 hrs exposure were 0.1533, 0.0313 and 0,0618 µg/ml respectively (Figure 7). We continued with concentrations ranged from 0.006 µg/ml to 6 µg/ml for our further *in vitro* experiments. Next, we performed cell proliferation and crystal violet assays. As depicted in Figure 8 to 10, Haprolid treatment suppressed cell proliferation of Hep3B, Huh-7 and HepG2 cell lines in a dose and time-dependent manner.

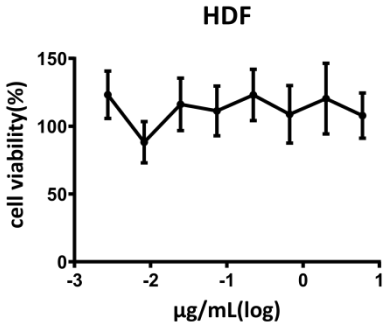

Figure 6. The effect of Haprolid on HDF cells. HDF (human dermal fibroblast) cells were treated with increasing concentration of Haprolid (0,001 to 18 µg/ml) for 96 hrs. WST-1 assay was performed to analyze cellular viability, DMSO was used as negative control. Data represent means ± SEM of at least three independent experiments.

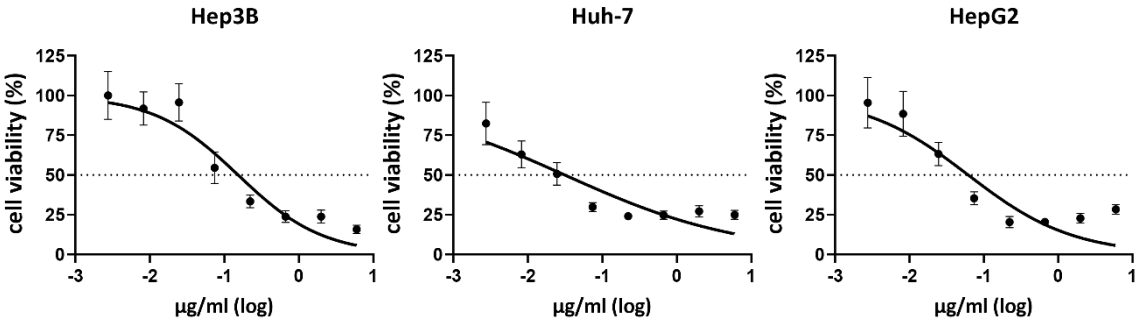

Figure 7. Cytotoxic effect of Haprolid (IC50) on HCC cells: Hep3B, Huh-7 and HepG2 cells were treated for 96 hrs with increasing concentrations of Haprolid (0,001 to 18 µg/ml). WST-1 assay was performed to analyze cellular viability, DMSO was used as negative control. Data represent means ± SEM of at least three independent experiments.

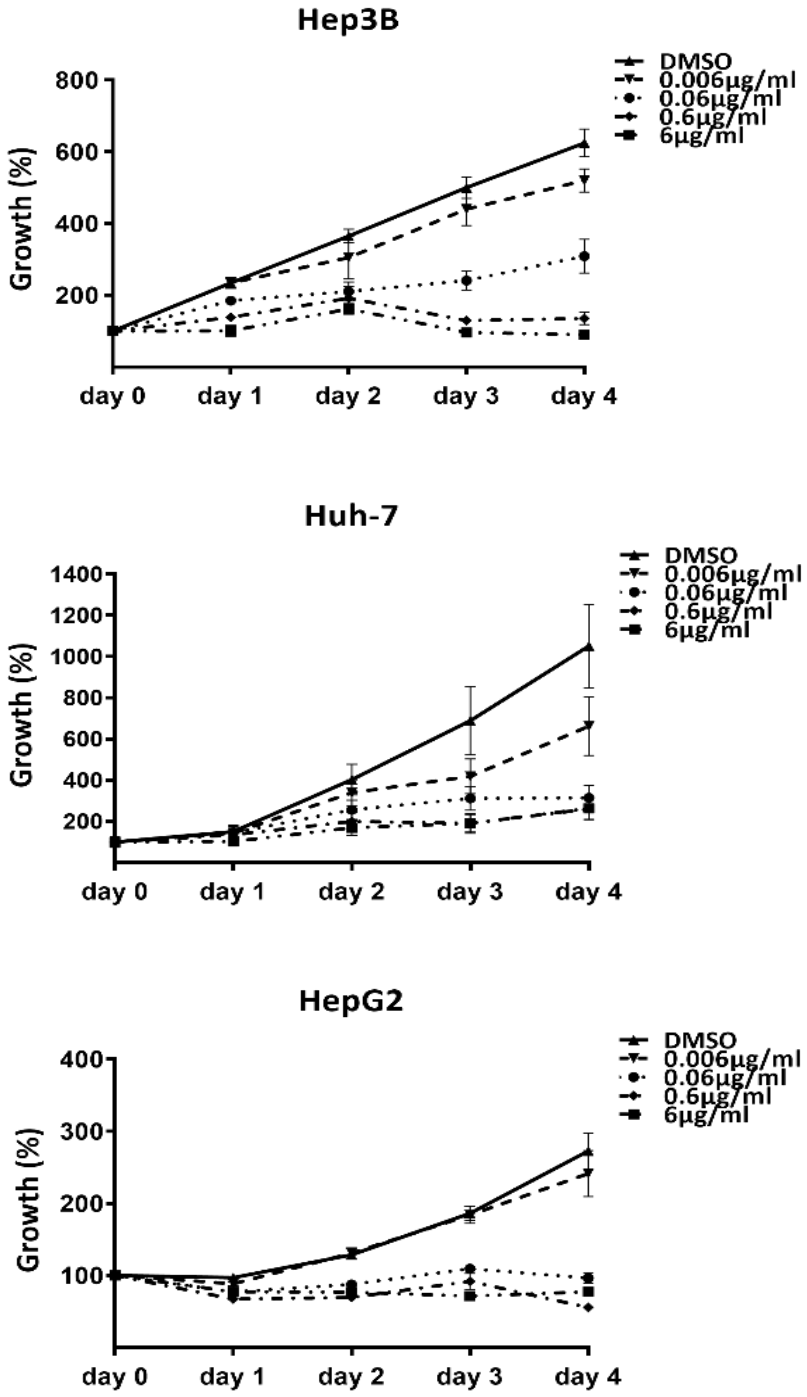

Figure 8. Haprolid treatment inhibits proliferation of human HCC cells. Cell proliferation of HCC cells treated with the indicated concentrations of Haprolid or DMSO measured by WST-1 assay. The relative cell number was normalized with the control. Data represent means ± SEM of at least three independent experiments.

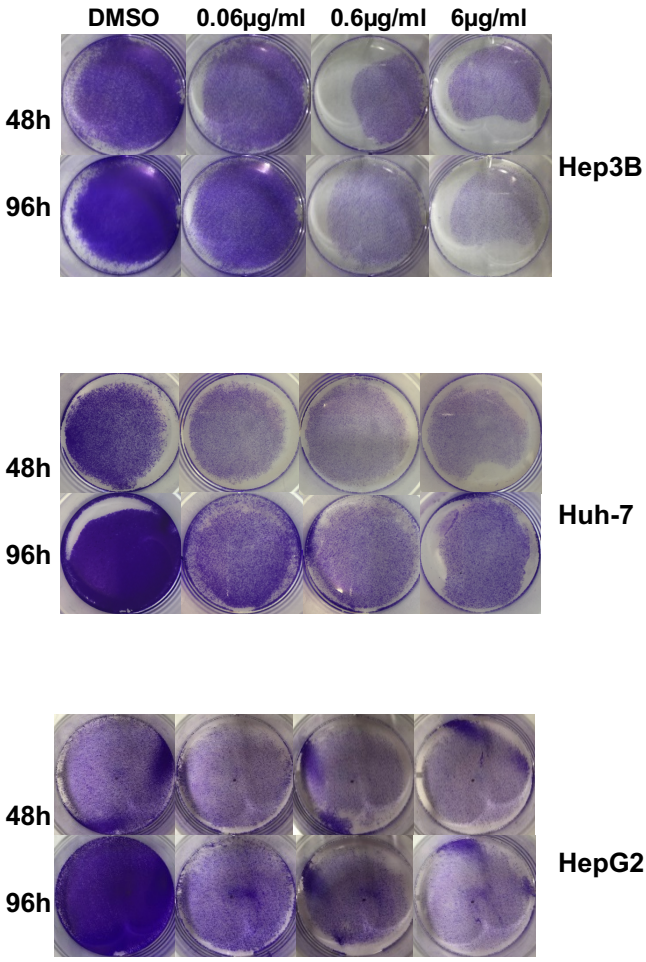

Figure 9. Crystal violet assay. HCC cells were fixed and stained with crystal violet 48 hrs and 96 hrs after Haprolid treatment.

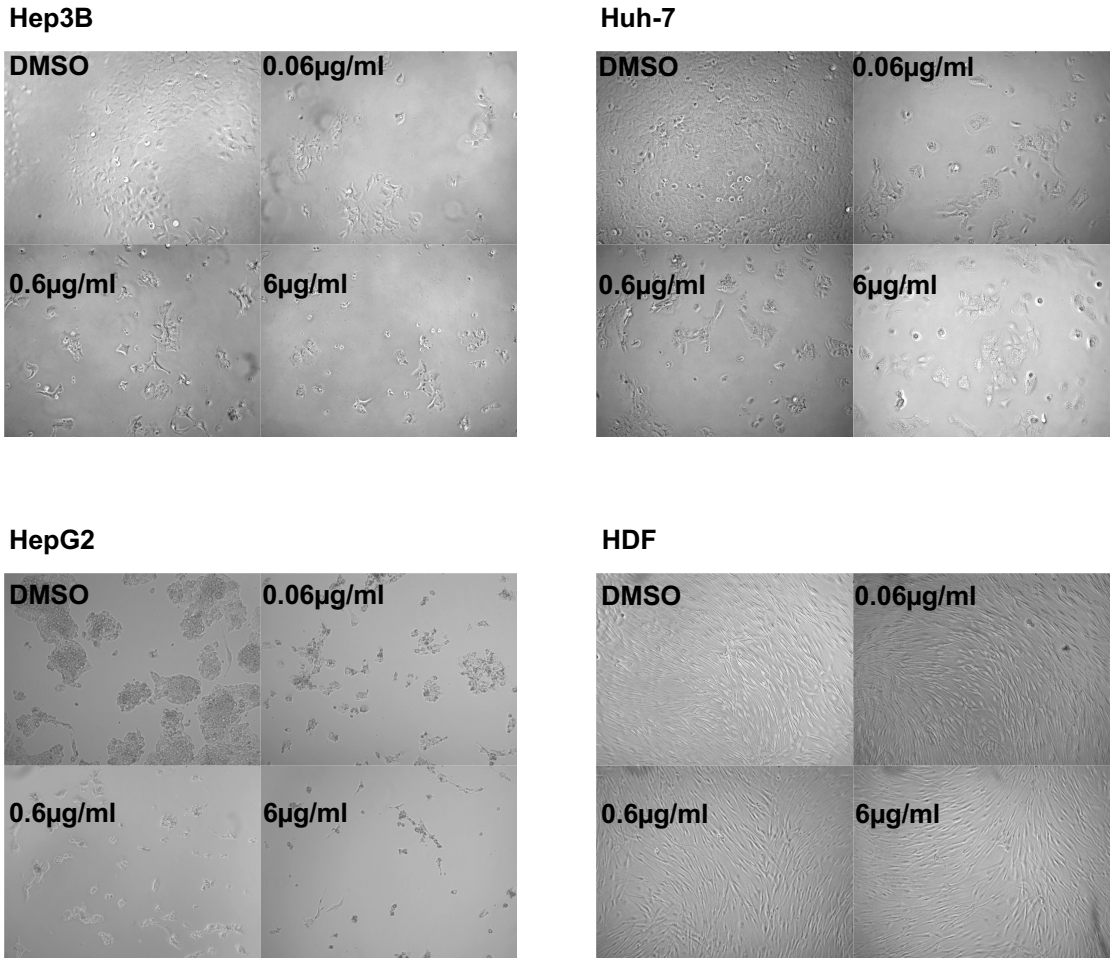

Figure 10. Differential cytotoxicity between HCC cells and human fibroblast cells. Hep3B, Huh-7, HepG2 and HDF cells were seeded in 96-well plates and treated with Haprolid (0.06, 0.6 and 6 µg/ml) or DMSO and corresponding light microcope pictures (100 X magnification) show treatment results after 96 hrs.

Furthermore, we examined the effect of Haprolid on the cell motility by employing wound healing and Matrigel transwell chamber assays. For all cell lines, significant inhibition of wound closure was seen after Haprolid treatment (Figure 11). Haprolid significantly reduced the number of invasive cells as illustrated in Figure 12. Thus, treatment with Haprolid can effectively suppress the migration and invasion in human HCC cells. Furthermore, we explored an *in vitro* three-dimensional tumor spheroid model to mimic physiologic tissue's microenvironment for investigating drug efficiency of Haprolid. As we can see in Figure 13 and 14, these results further confirmed that Haprolid treatment significantly inhibited the growth and invasion of spheroid in Hep3B and Huh-7 cells. Our experiments showed that incubation of the Huh-7 cell line with Haprolid for 10 days suppressed the growth of spheroid size but with no regression, whereas similar incubation of the Hep3B cell line readily resulted in reduction of tumor spheroid size at concentrations 0.6 μg/ml as early as 4 days. Taken together, these data suggest that Haprolid can significantly inhibit proliferation, migration and invasion of human HCC cells. In general, Hep3B cells shows overall stronger inhibitory effect under Haprolid treatment compared to Huh-7 and HepG2 cells.

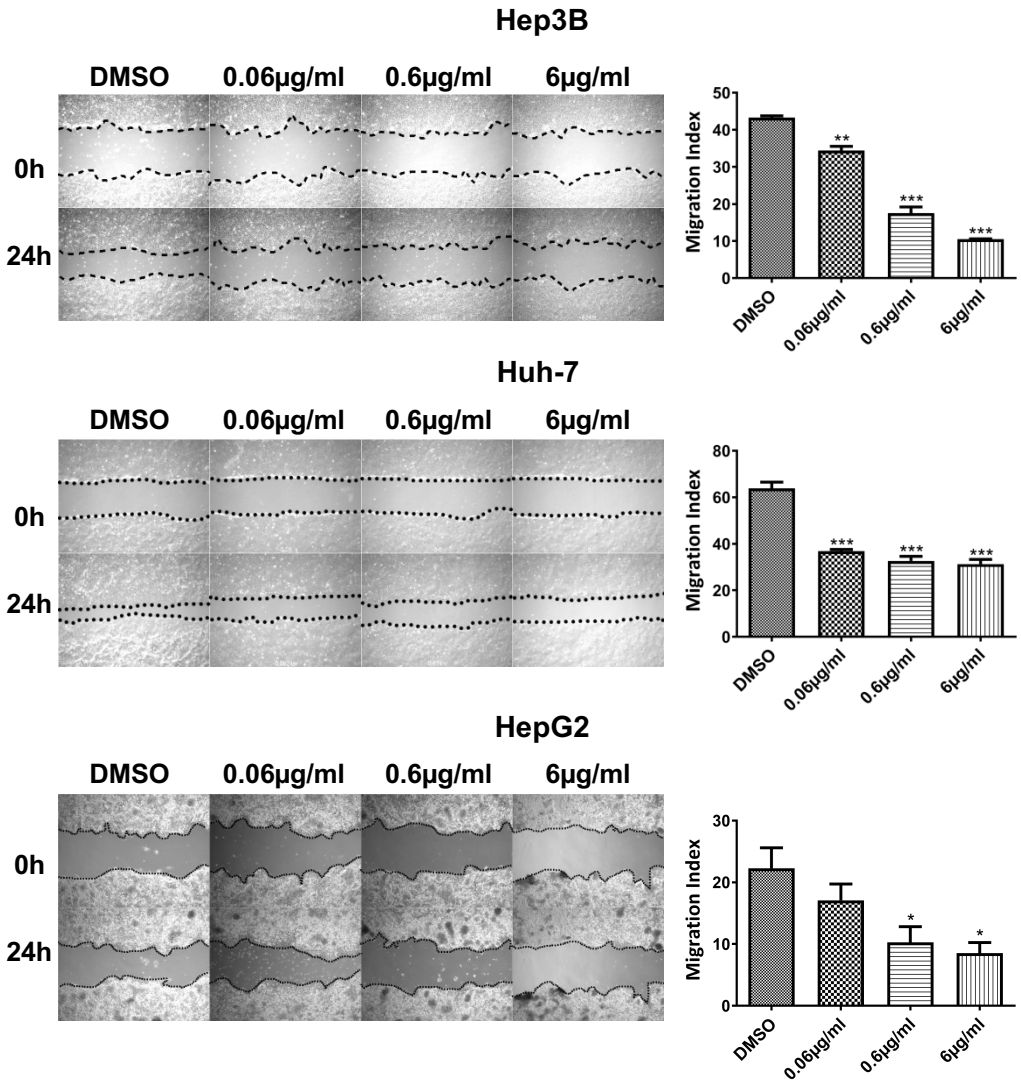

Figure 11. Inhibition of migration in Haprolid-treated HCC cells. Wound healing assay was performed for Hep3B, Huh-7 and HepG2 cells after Haprolid (0.06, 0.6 and 6 µg/ml) treatment. The dotted lines represent edges of the wound. Photographs were taken at 0 and 24 hrs under light microscope (40 X magnification). The migration index was calculated as described in materials and methods and plotted in bar graphs. Data represent means ± SEM of at least three independent experiments. *P < 0.05, **P < 0.01, ***P < 0.001, ****P < 0.0001.

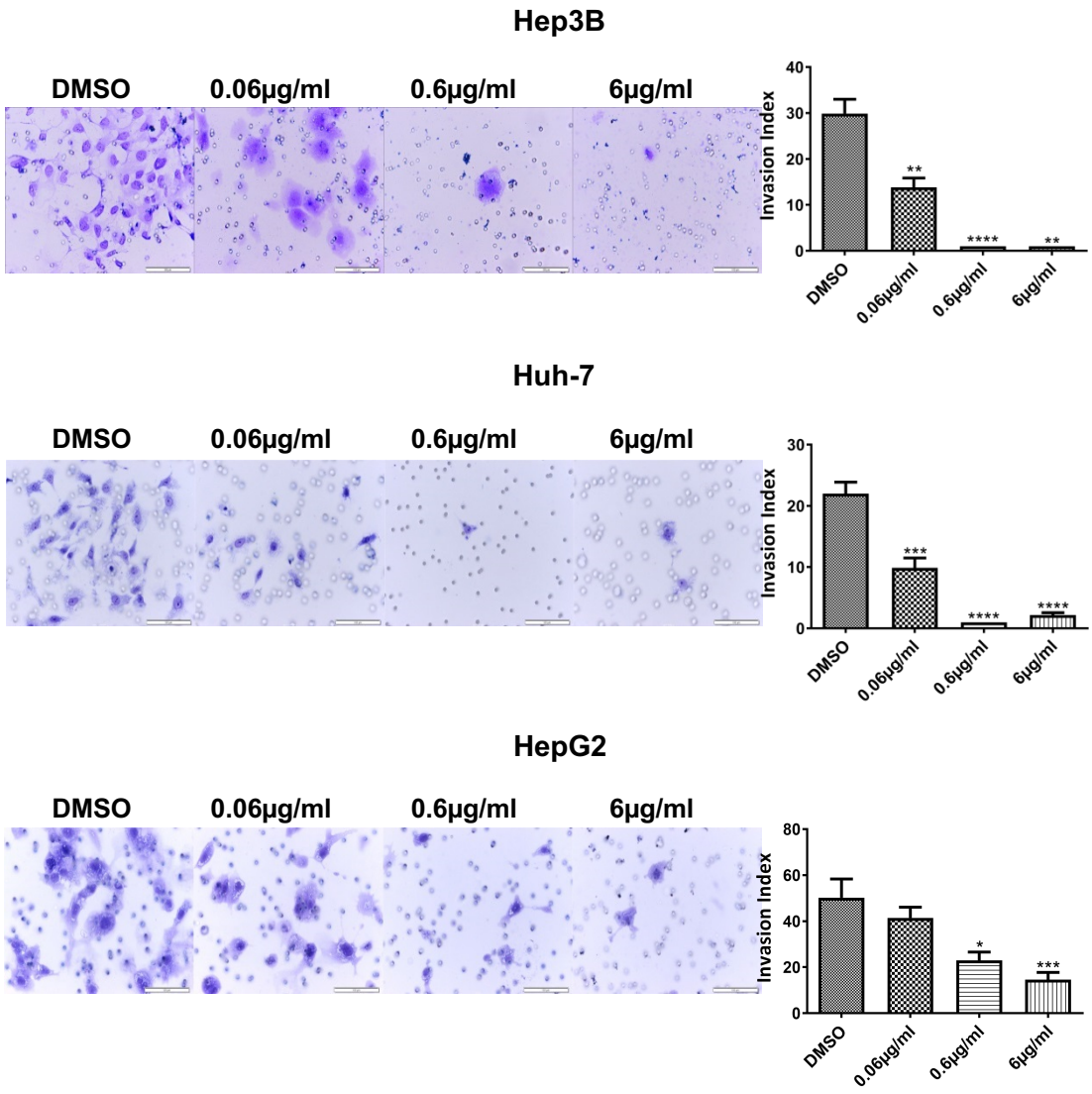

Figure 12. Inhibition of invasion in Haprolid-treated HCC cells. HCC cells were seeded in matrigel transwell invasion chambers and treated with indicated concentrations of Haprolid for 48 hrs to investigate the effect on invasiveness. The number of cells that invaded through the membrane was determined under light microscope (200 X magnification). Invasion index was calculated as described in materials and methods and plotted in bar graphs. Data represent means ± SEM of at least three independent experiments. *P < 0.05, **P < 0.01, ***P < 0.001, ****P < 0.0001.

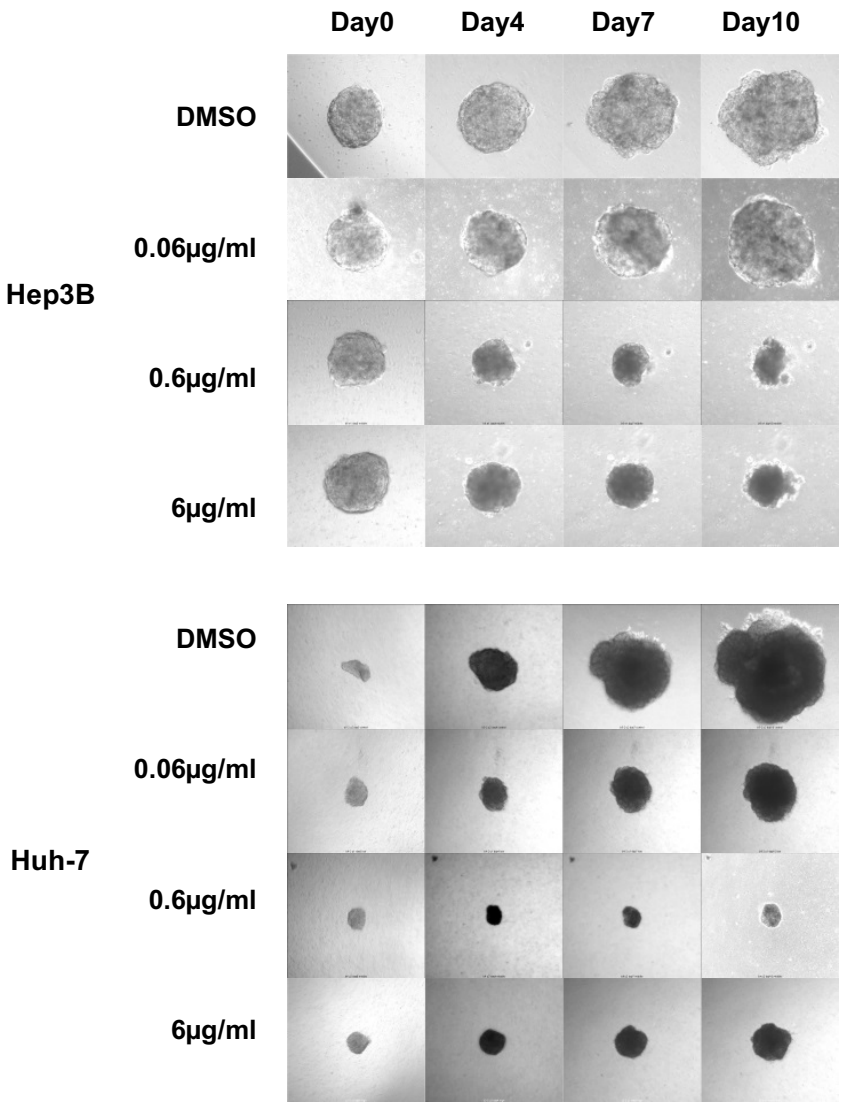

Figure 13. Haprolid treatment inhibits tumor spheroids growth and invasion. Three dimensional tumor spheroid assay was performed to evaluate effects of Haprolid on HCC cell proliferative and invasive ability in extracellular matrix-like environment. The representative images of spheroids are shown.

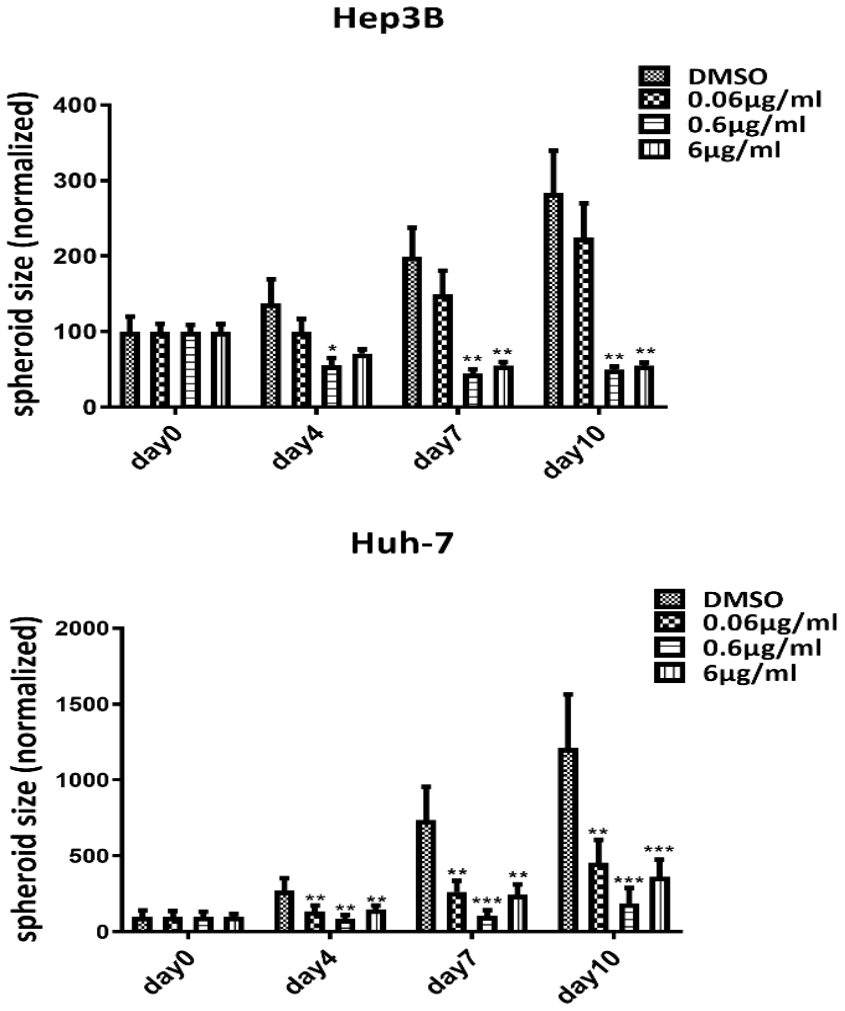

Figure 14. Quantification of tumor spheroids size. The changes of spheroids size were monitored and quantified up to 10 days and plotted in bar graphs. Data represent means ± SEM of at least three independent experiments. *P < 0.05, **P < 0.01, ***P < 0.001, ****P < 0.0001.

3.2 Haprolid treatment impairs epithelial-mesenchymal transition (EMT) in HCC cells

Moreover, based on the findings that Haprolid treatment significantly inhibited the HCC cell motility, we continued to investigate the impact of Haprolid in EMT. At a molecular level, EMT is frequently assessed by changes in the expression patterns of putative EMT markers: the acquisition of mesenchymal markers, including cytoskeletal protein Vimentin and cell surface protein N-cadherin, and

the downregulation of epithelial markers, such as the junction protein E-cadherin [82, 83]. In order to examine whether Haprolid can attenuate EMT *in vitro*, we treated HCC cells with increasing concentrations of Haprolid for 96 hrs and compared to DMSO as a control. In both Hep3B and Huh-7 cells, Haprolid treatment resulted in decreased expression of the mesenchymal proteins N-cadherin and Vimentin as assessed by Western Blot (Figure 15). However, the expression of epithelial protein E-cadherin was only slightly upregulated (Figure 15). Thus, we next checked the expression of Snail, a zinc-finger EMT transcription factor that functions as a potent repressor of E-cadherin [84]. As shown in Figure 15, the level of Snail was markedly diminished after Haprolid treatment. These changes indicate that Haprolid treatment partially impairs EMT in HCC cells.

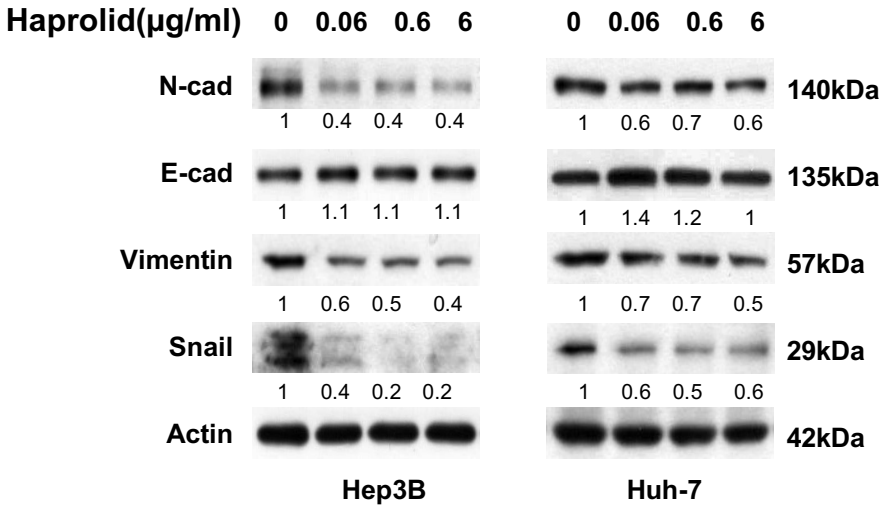

Figure 15. Haprolid partially impairs epithelial mesenchymal transition (EMT) in human HCC cells. Hep3B and Huh-7 cells were treated with DMSO or Haprolid (0.06, 0.6 and 6 μg/ml) for 96 hrs. The expressions of EMT markers (N-cadherin, E-cadherin, Vimentin and Snail) were analyzed by immunoblotting. Western blotting bands were quantified by Image J and normalized to their respective β- actin then compared with vehicle-treated controls.

3.3 Haprolid treatment inhibits G1/S transition and induces cell cycle arrest in HCC cells.

To clarify the underlying mechanisms for the anti-proliferative effect of Haprolid, cell cycle and apoptosis were analyzed. Fluorescence-activated cell sorting (FACS) analysis was conducted to determine the cell cycle profiles of all three HCC cell lines when exposed to increasing concentrations of Haprolid for 48 hrs and 96 hrs. Figure 16 shows the distribution of cells in various phases of the cell cycle. The percentages of the cell cycle distribution across the population are listed in Table 1, and the graphical representations of the sub-G1-, G1-, S- and G2-M-values are shown in Figure 17. In Huh-7 and HepG2 cells, Haprolid treatment caused a significant increase in the number of cells in G1 phase compared to controls, which was accompanied by a decrease in the number of S and G2-M phase cells, indicating a block of G1/S transition (Figure 16 and 17). Although Hep3B cells also accumulated in the G1 phase at lower concentration (0.06 µg/ml), at higher concentrations of the compound treatment, a large proportion of the cells accumulated in the sub-G1 phase, suggesting an induction of apoptosis, which was also evidenced by following experiments. Overall, Haprolid treatment inhibits the G1/S transition and results in markedly cell cycle arrest in all tested cell lines. Moreover, Haprolid treatment leads to growth arrest later on induces considerable apoptosis in Hep3B cells.

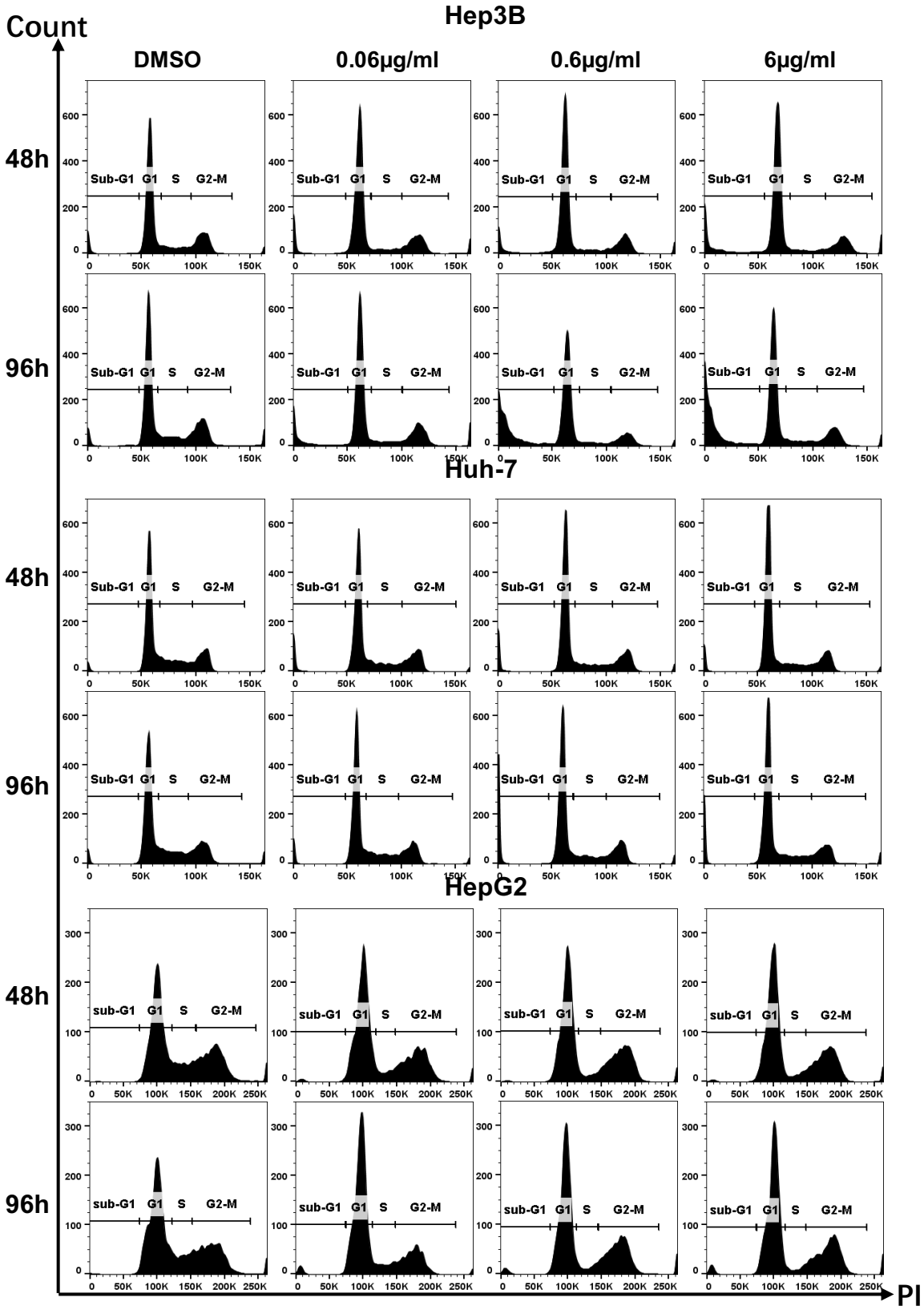

Figure 16. Haprolid treatment inhibits G1/S transition and induces cell cycle arrest in HCC cells. HCC cells were treated with vehicle (DMSO) or increasing concentrations of Haprolid for 48 hrs and 96 hrs, fixed and stained with propidium iodide (PI) and subjected to flow cytometric analysis. Representative cell cycle histograms are presented.

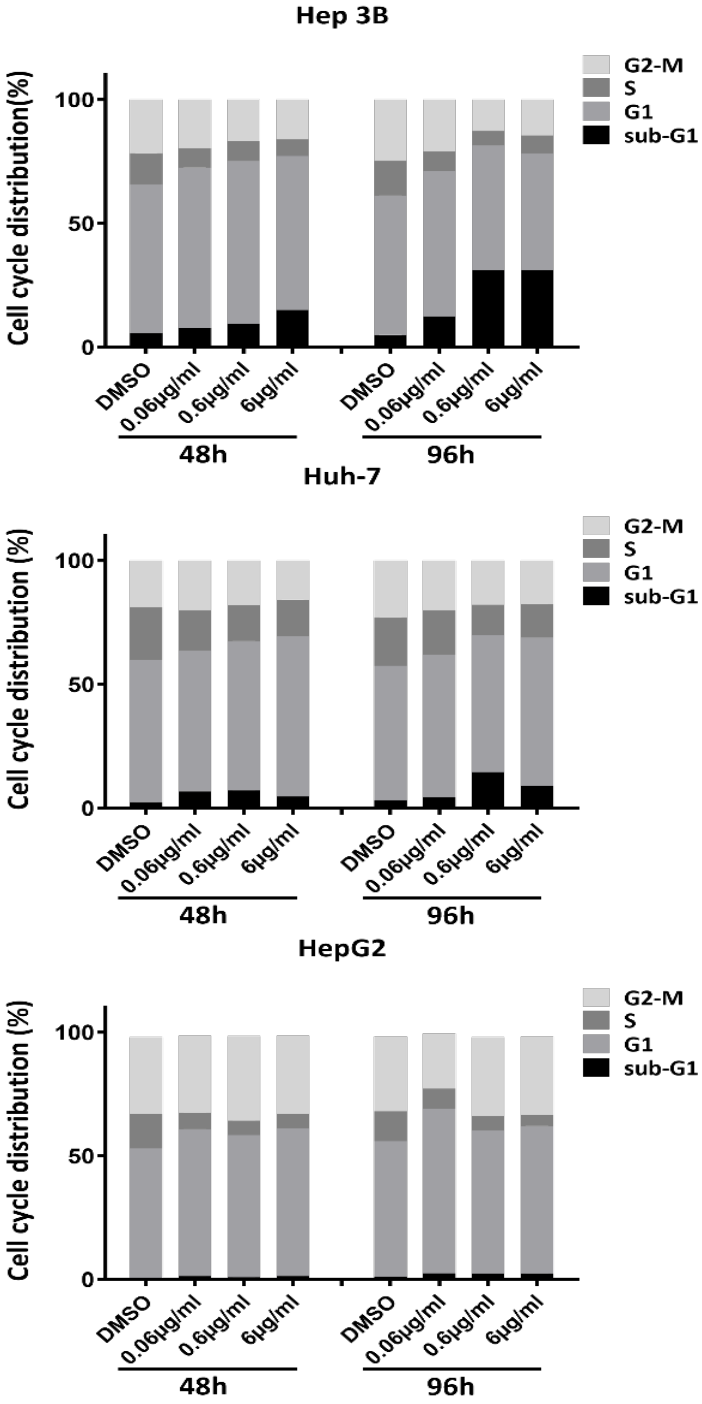

Figure 17. Cell cycle distribution after Haprolid treatment. HCC cells were treated with vehicle (DMSO) or increasing concentrations of Haprolid for 48 hrs and 96 hrs, fixed and stained with propidium iodide (PI) and subjected to flow cytometric analysis. Cell cycle distribution in various phases is determined and shown

Table 1. The percentages of the cell cycle distribution across the sub-G1-, G1-, S- and G2-M-phases in control- and Haprolid-treated HCC cells

Hep3B (%)				
48h	sub-G1	G1	S	G2-M
DMSO	5,60	60,15	12,64	21,61
0.06µg/ml	7,65	64,94	7,61	19,80
0.6µg/ml	9,29	65,83	7,99	16,89
6µg/ml	14,93	62,19	6,71	16,16
96h	sub-G1	G1	S	G2-M
DMSO	5,02	56,20	14,00	24,78
0.06µg/ml	12,17	59,00	7,89	20,94
0.6µg/ml	31,03	50,44	5,79	12,74
6µg/ml	31,20	47,05	7,22	14,53
Huh-7 (%)				
48h	sub-G1	G1	S	G2-M
DMSO	2.33	57.48	21.30	18.89
0.06µg/ml	6.63	56.95	16.30	20.12
0.6µg/ml	7.16	60.34	14.28	18.22
6µg/ml	4.67	64.60	14.96	15.77
96h	sub-G1	G1	S	G2-M
DMSO	3.08	54.40	19.57	22.95
0.06µg/ml	4.38	57.57	17.91	20.14
0.6µg/ml	14.53	55.28	12.30	17.89
6µg/ml	8.92	59.90	13.65	17.52
HepG2 (%)				
48h	sub-G1	G1	S	G2-M
DMSO	0.65	52.3	14	31.1
0.06µg/ml	1.31	59.5	6.69	31.2
0.6µg/ml	0.91	57.4	5.94	34.2
6µg/ml	1.32	59.8	5.8	31.6
96h	sub-G1	G1	S	G2-M
DMSO	1.09	54.8	12.1	30.3
0.06µg/ml	2.45	66.6	8.07	22.3
0.6µg/ml	2.11	58.1	5.73	32
6µg/ml	2.37	59.7	4.29	31.8

To confirm cell cycle analysis data, we investigated the time-course expression and activation of cell cycle checkpoint proteins via western blot (Figure 18). Consistent with the inhibition of G1-to-S phase progression we found dynamically decreased cyclin A and cyclin B expression in response to Haprolid treatment in all cell lines.

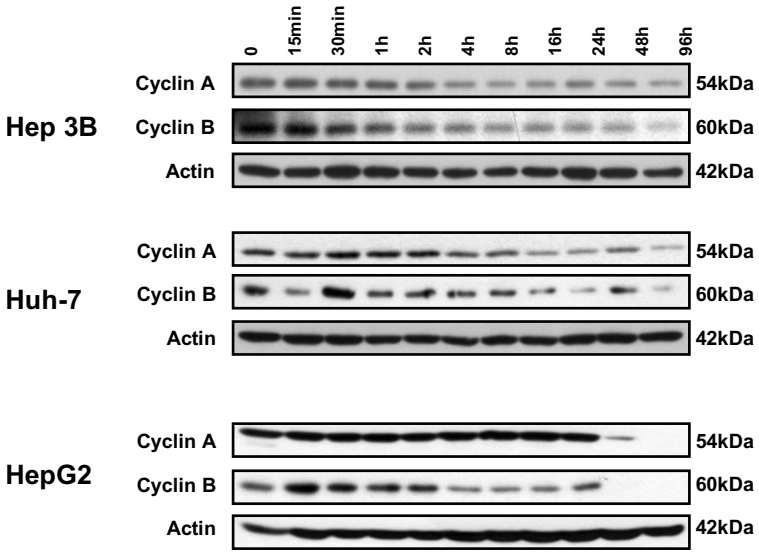

Figure 18. Kinetic analysis of cyclin A and cyclin B after Haprolid treatment. Cyclin A and B expression was measured by western blotting. Images representative of at least three independent experiments are shown.

3.4 Haprolid partially induces apoptosis in HCC cells

Additionally, Annexin V and PI staining was performed on live cells to determine whether the cell-cycle arrest phenotype was associated with the induction of apoptosis. We noticed that exposure to Haprolid dose dependently increased apoptotic cells in Hep3B cell line (Figure 19-21). Moreover, proteolytic cleavage of poly (ADP ribose) polymerase (PARP) as an indicative marker of apoptosis was evaluated by quantitative measurement [85]. Immunoblotting revealed distinct PARP cleavage after Haprolid treatment in Hep3B cells (Figure 19-21). Interestingly, Huh-7 and HepG2 cells are not sensitive to the apoptosis-inducing effects of Haprolid (Figure 19-21). These results confirm our previous studies and suggest that Huh-7 and HepG2 cells are relative resistance of apoptosis and mainly undergo cell-cycle arrest under Haprolid treatment, while Haprolid induces noticeable apoptotic cell death in Hep3B cells following cytostatic effect.

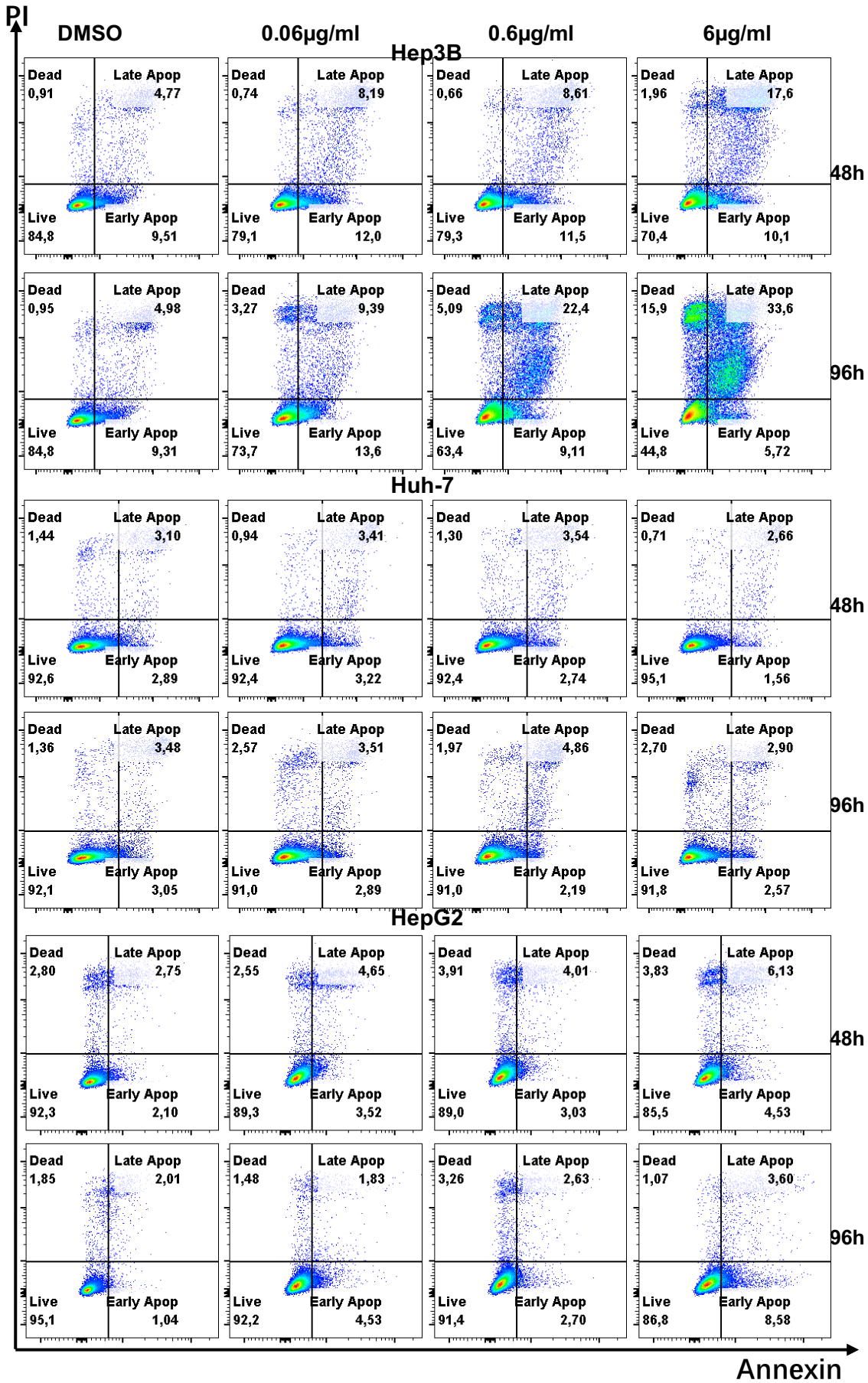
PI
DMSO
0.06µg/ml
0.6µg/ml
6µg/ml
Hep3B
48h
Dead 0,91 Late Apop 4,77 Live 84,8 Early Apop 9,51
Dead 0,74 Late Apop 8,19 Live 79,1 Early Apop 12,0
Dead 0,66 Late Apop 8,61 Live 79,3 Early Apop 11,5
Dead 1,96 Late Apop 17,6 Live 70,4 Early Apop 10,1
96h
Dead 0,95 Late Apop 4,98 Live 84,8 Early Apop 9,31
Dead 3,27 Late Apop 9,39 Live 73,7 Early Apop 13,6
Dead 5,09 Late Apop 22,4 Live 63,4 Early Apop 9,11
Dead 15,9 Late Apop 33,6 Live 44,8 Early Apop 5,72
Huh-7
48h
Dead 1,44 Late Apop 3,10 Live 92,6 Early Apop 2,89
Dead 0,94 Late Apop 3,41 Live 92,4 Early Apop 3,22
Dead 1,30 Late Apop 3,54 Live 92,4 Early Apop 2,74
Dead 0,71 Late Apop 2,66 Live 95,1 Early Apop 1,56
96h
Dead 1,36 Late Apop 3,48 Live 92,1 Early Apop 3,05
Dead 2,57 Late Apop 3,51 Live 91,0 Early Apop 2,89
Dead 1,97 Late Apop 4,86 Live 91,0 Early Apop 2,19
Dead 2,70 Late Apop 2,90 Live 91,8 Early Apop 2,57
HepG2
48h
Dead 2,80 Late Apop 2,75 Live 92,3 Early Apop 2,10
Dead 2,55 Late Apop 4,65 Live 89,3 Early Apop 3,52
Dead 3,91 Late Apop 4,01 Live 89,0 Early Apop 3,03
Dead 3,83 Late Apop 6,13 Live 85,5 Early Apop 4,53
96h
Dead 1,85 Late Apop 2,01 Live 95,1 Early Apop 1,04
Dead 1,48 Late Apop 1,83 Live 92,2 Early Apop 4,53
Dead 3,26 Late Apop 2,63 Live 91,4 Early Apop 2,70
Dead 1,07 Late Apop 3,60 Live 86,8 Early Apop 8,58
Annexin

Figure 19. Apoptotic effect of Haprolid on HCC cells. HCC cells were treated with DMSO or Haprolid (0.06, 0.6 and 6 μg/ml) for 48 hrs and 96 hrs, the level of apoptosis was measured by staining with Annexin V and PI using flow cytometry. Representative FACS measurements are presented.

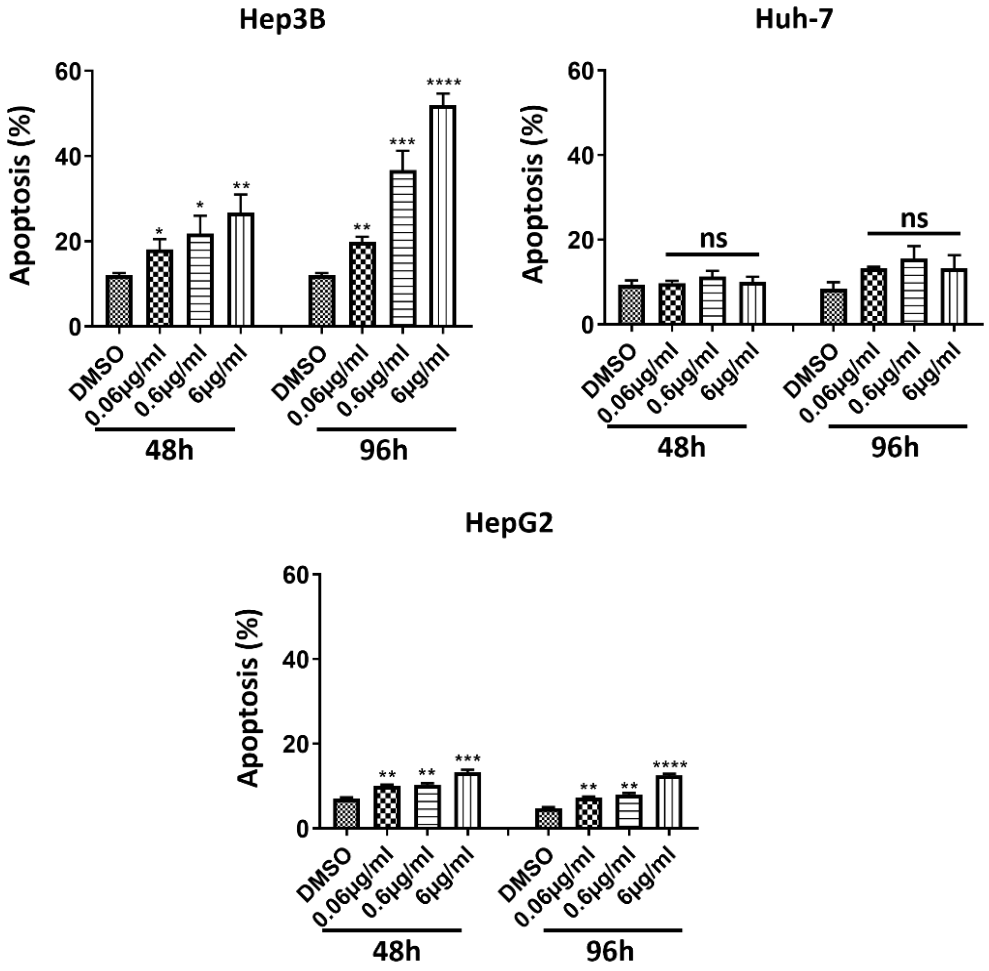

Figure 20. HCC cells were treated with DMSO or Haprolid (0.06, 0.6 and 6 μg/ml) for 48 hrs and 96 hrs, the level of apoptosis was measured by staining with Annexin V and PI using flow cytometry. The apoptotic positive cells were calculated and plotted in bar graph. Data represent means ± SEM of at least three independent experiments. *P < 0.05, **P < 0.01, ***P < 0.001, ****P < 0.0001.

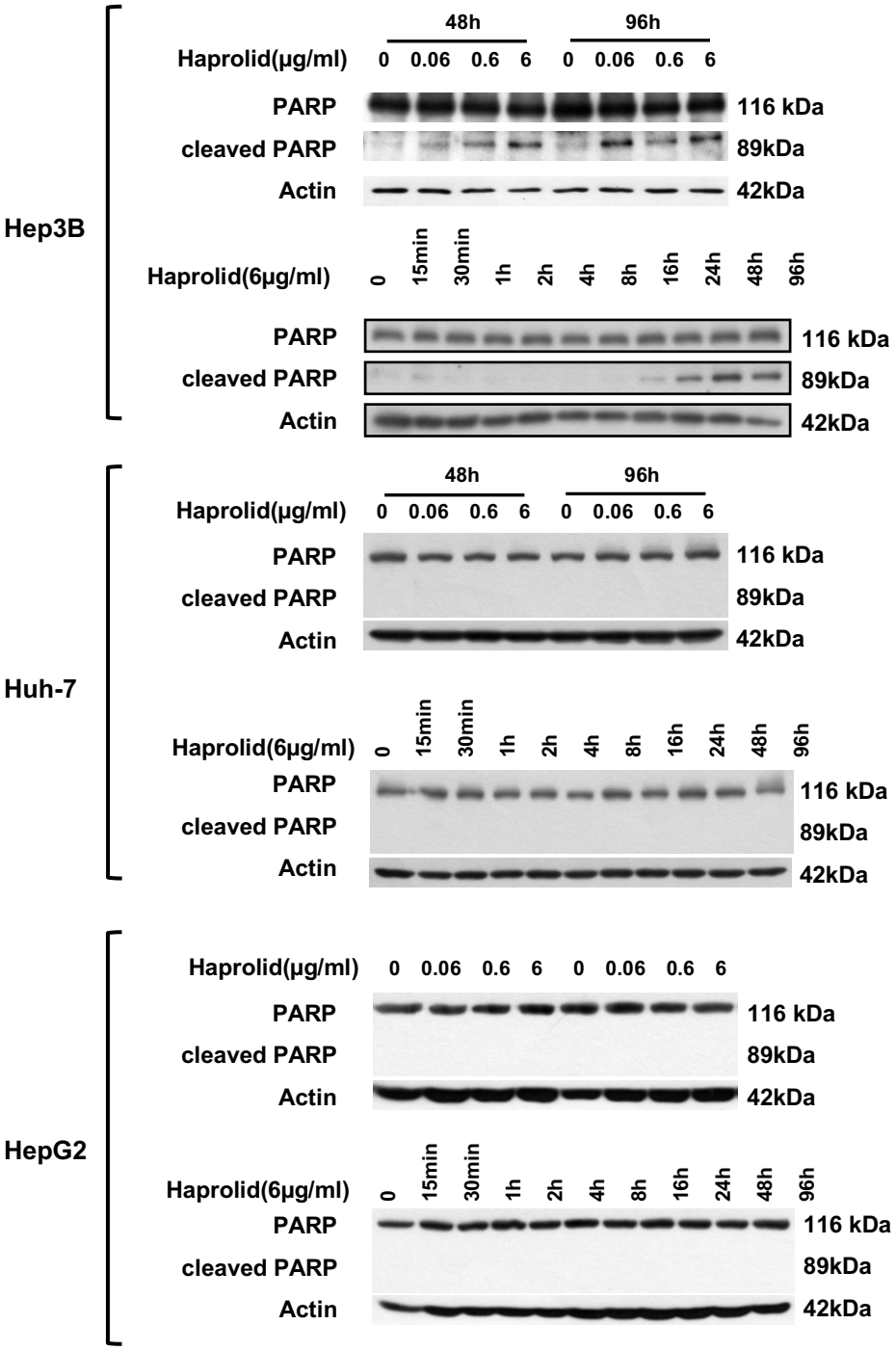

Figure 21. Expression of PARP and cleaved PARP (a marker for apoptosis) after Haprolid treatment was measured by western blotting.

3.5 Dual inhibition of Rb/E2F and Akt/mTOR pathways by Haprolid

To investigate the mechanism of Haprolid-induced cell cycle arrest and apoptosis, we next examined the expression levels of checkpoint proteins in the G1/S transition and cell cycle modulation factors at the G1/S boundary by western blot analysis. First, we checked the expression level of retinoblastoma protein Rb which is a universal cell cycle regulator with a central role in controlling the commitment of a cell to initiate DNA replication and division [44]. Figure 22 demonstrated that – despite of the Rb-deficient Hep3B cell line - after Haprolid treatment the level of p-Rb expression decreased and Rb changed from the hyperphosphorylated form to the hypophosphorylated form in both Huh-7 and HepG2 cell lines. Moreover, the protein level of E2F-1, the downstream target of Rb, which is the essential transcription factor that regulates cell cycle progression and stimulates proliferation [86], was considerably inhibited after exposure to Haprolid in all three HCC cells. Inhibition of Rb phosphorylation and reduction in levels of free E2F-1 appear to play an important role in HCC growth arrest. Haprolid treatment also resulted in a noticeable downregulation of cyclin-dependent kinase 2 (CDK2) in all three HCC cells, and upregulation of cyclin-dependent kinase inhibitors (CDKIs), p21 and p27 in both Hep3B and HepG2 cells. We also found upregulation of p21 but not p27 in Huh-7 cells (Figure 22). Immunoblot for phospho-Ser10-histone H3, a specific marker of mitosis, was also applied to confirm our previous data regarding cell cycle arrest. As expected, there was a remarkable down-regulation in p-histone H3 expression in all tested HCC cells (Figure 22). Taken together, Haprolid induces G1/S phase arrest in HCC cells through contributing to the modulation of cell cycle regulatory proteins and inactivation of the Rb/E2F pathway.

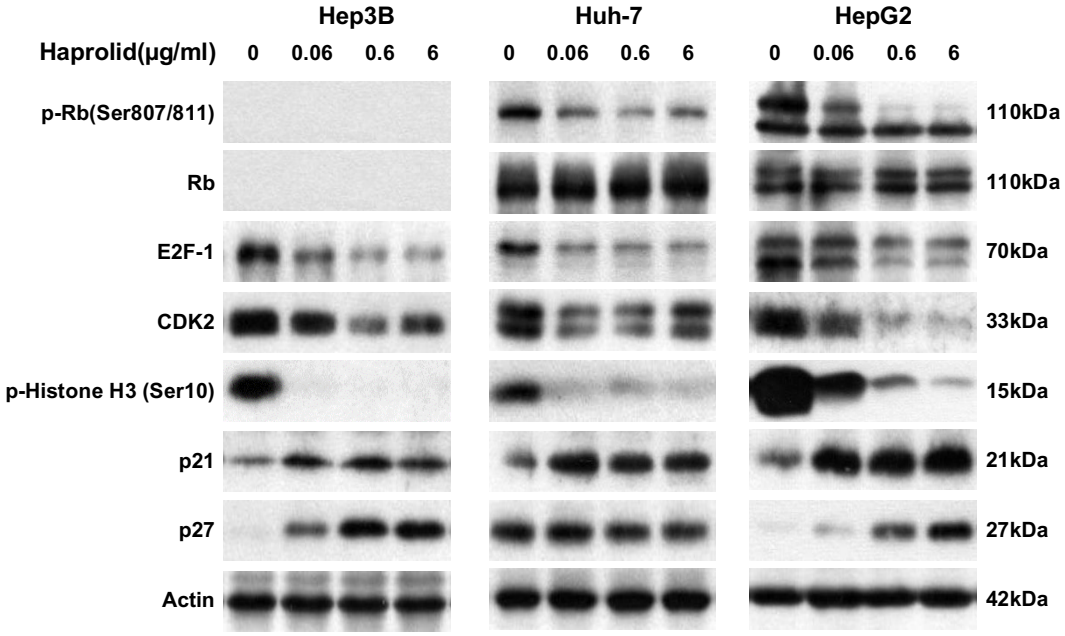

Figure 22. Inhibition of Rb/E2F pathways by Haprolid. Hep3B, Huh-7 and HepG2 cells were treated with increasing concentrations of Haprolid or DMSO for 96 hrs. Cell lysates were analyzed by western blotting with antibodies against indicated proteins. β-actin is shown as a loading control. Images representative of at least three independent experiments are shown.

The Akt/mTOR signaling pathway is pivotal to cellular growth and proliferation as well as survival [53]. This pathway is activated in a subset of patients with HCC and plays a critical role in HCC carcinogenesis [43]. Therefore, we also analyzed the activity of Akt and mTOR. Haprolid treatment significantly decreased the Akt activity at high concentrations: the expression of both total Akt and p-Akt at Ser473, a central regulator of cell survival, were downregulated (Figure 23). In contrast, low-dose treatment (0.06 μg/ml) with Haprolid resulted in weakly increased p-Akt levels in Hep3B and Huh-7 cells, which indicated a dose dependent differential response to Haprolid treatment. Subsequently, decreased p-mTOR levels were detected in Hep3B and Huh-7 cells whereas no detectable changes were observed in HepG2 cells (Figure 23). Finally, phosphorylation of

downstream Akt/mTOR targets, S6K and S6 [87, 88], were significantly reduced upon Haprolid treatment in all studied cells (Figure 23). Our results imply that Haprolid inhibits cell growth and induces apoptotic cell death in HCC cells through interfering with the Akt/mTOR signaling pathway. Overall, these studies provide a molecular basis to understand the signaling mechanisms through which Haprolid influences the cell growth and proliferation in HCC.

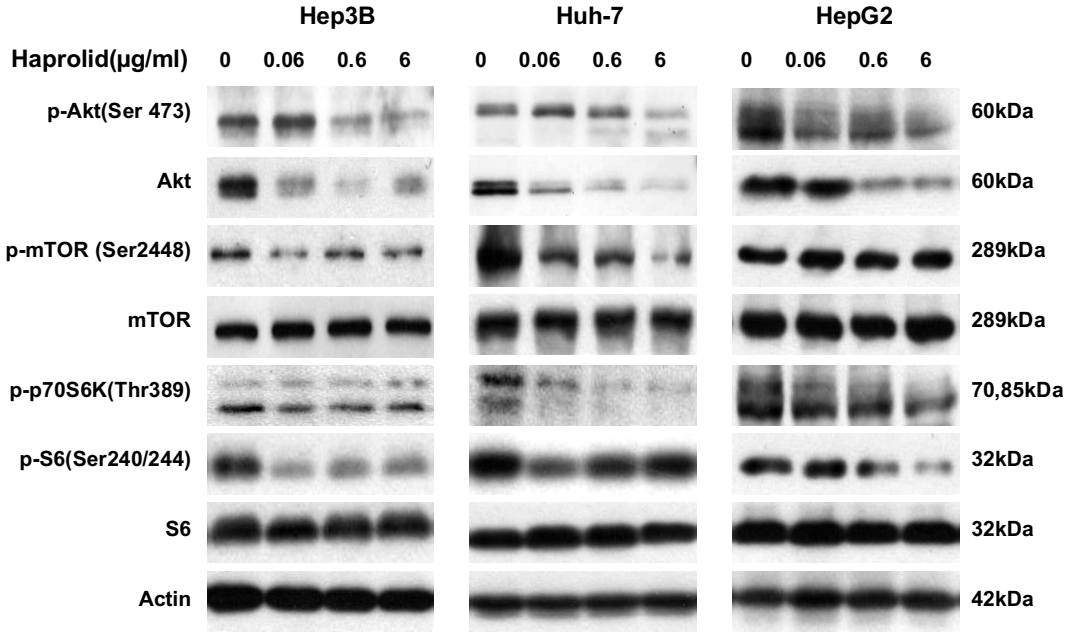

Figure 23. Inhibition of Akt/mTOR pathways by Haprolid. Hep3B, Huh-7 and HepG2 cells were treated with increasing concentrations of Haprolid or DMSO for 96 hrs. Cell lysates were analyzed by western blotting with antibodies against indicated proteins. β-actin is shown as a loading control. Images representative of at least three independent experiments are shown.

3.6 Haprolid treatment inhibits tumor growth in NMRI-Foxn1^{nu} mice

To further evaluate the *in vivo* anti-tumor activity of Haprolid, we used a subcutaneous xenograft model with Hep3B cells. Hep3B cells were selected, because it was demonstrated to be the most sensitive to Haprolid of the three

tested cell lines. Mice with tumor xenografts were randomly assigned into two treatment groups and treatment was initiated when xenograft tumors reached a size of ~ 100mm^3. Figure 24 showed a representative image of tumors for control and Haprolid group (2 mg/kg). As shown in Figure 25, comparing with the control group, tumor growth in Haprolid group was significantly suppressed. In Figure 25c, from 2 weeks of treatment onwards, Haprolid induced a statistically significant inhibition of tumor growth ($P< 0.01$) compared to the control group. Over a 5-week period of Haprolid treatment, the mean tumor weight was 510.9 ± 84.7 mg compared with 858 ± 75.8 mg in the control group, indicating that the drug reduced tumor growth by 40.4 percent (Figure 25b). In addition, the total body weight during the entire experiments was not significant different between both groups and no side effects were noticed (Figure 26 and 27). Correspondingly, mice bearing Hep3B tumors which received Haprolid treatment exhibited decreased levels of Ki-67, Akt and p-S6 (Figure 28), as evidenced by IHC analysis. These results, in addition to those obtained *in vitro*, suggest that Haprolid is a potent inhibitor of HCC growth.

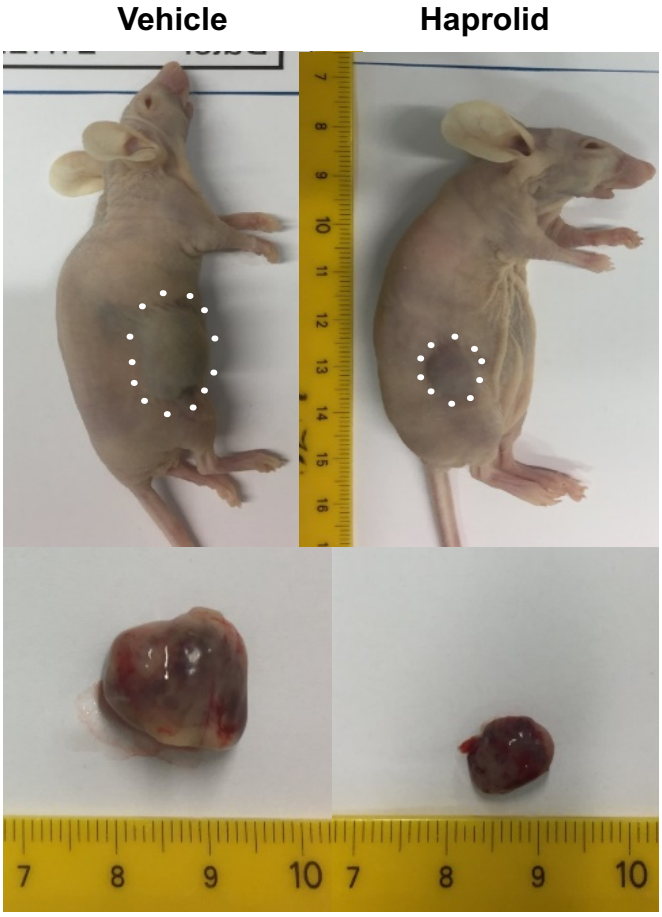

Figure 24. Representative image of tumors in control- and Haprolid-treated (2 mg/kg body weight) mice. Dotted lines sketch out tumors in the flanks.

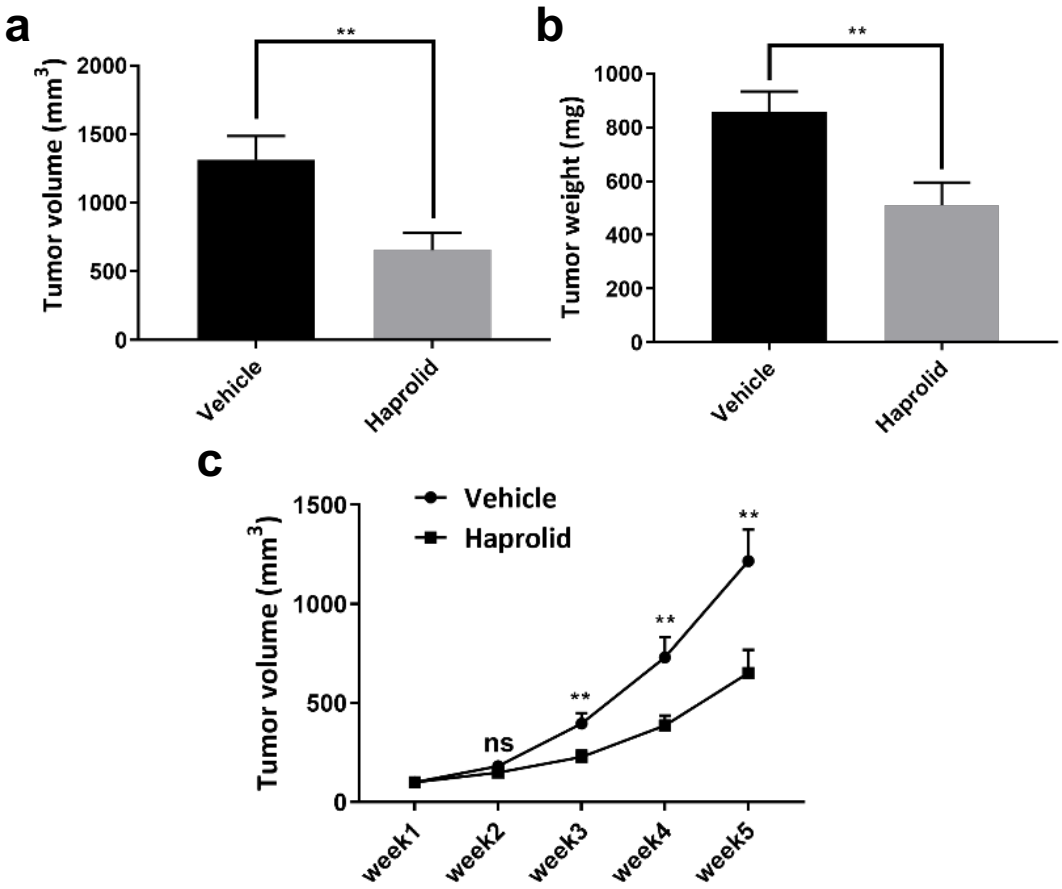

Figure 25. Effect of Haprolid on mice bearing Hep3B xenograft tumor. (a and b) Mean tumor volume and weight in control- and Haprolid-treated mouse groups (n ≥ 5 per group). (c) Tumor growth curves.

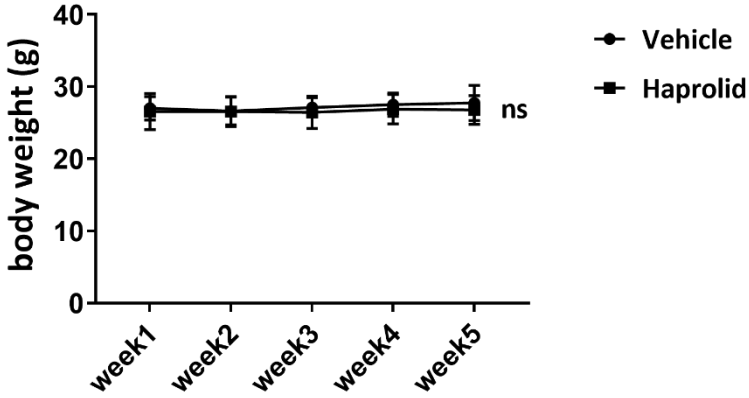

Figure 26. Body weight of control- and Haprolid-treated mice. Both groups showed stable body weight throughout the experiment.

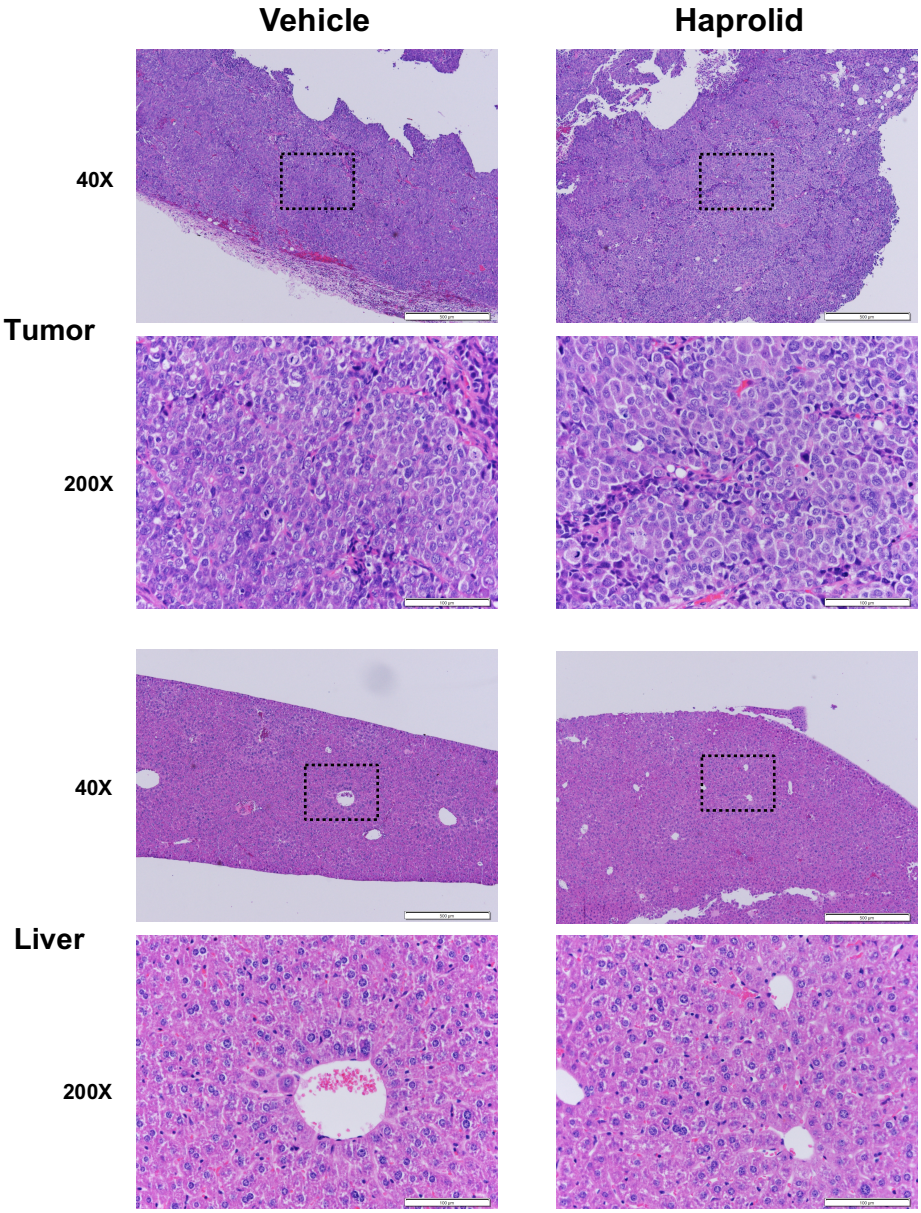

Figure 27. Evaluation of side effects of Haprolid in mice. H&E stainings of tumors and livers from control and Haprolid-treated mouse groups.

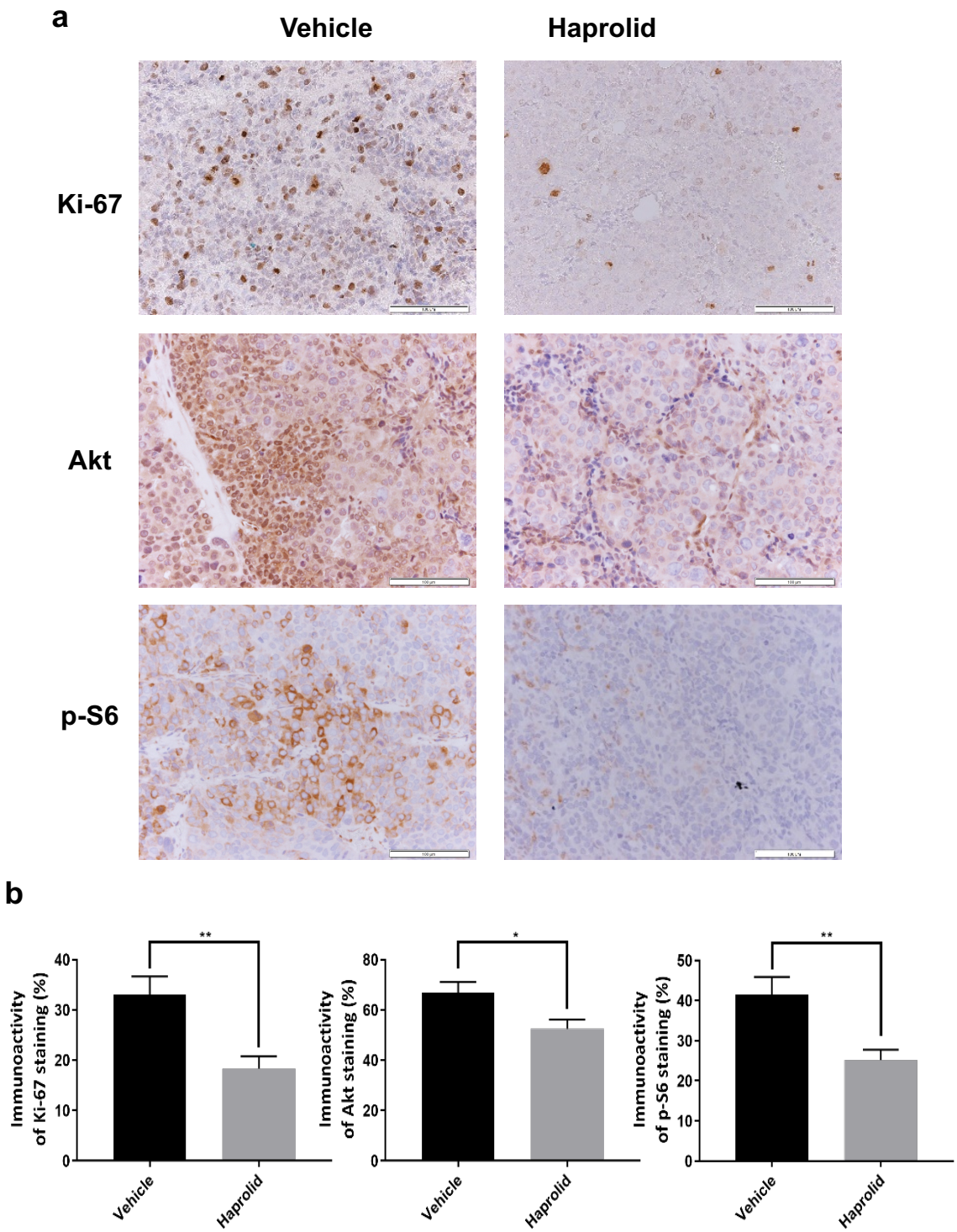

Figure 28. IHC staining of Ki67, Akt and p-S6 of xenograft tumor tissue. (a)Tumor tissue sections were stained with Ki67, Akt and p-S6. Representative IHC staining images were taken at 200 X magnification. (b) Immunostaining activity of Ki67, Akt and p-S6 was scored and plotted in bar gragh. Data represent means ± SEM of at least three independent experiments. *P < 0.05, **P < 0.01, ***P < 0.001, ****P < 0.0001.

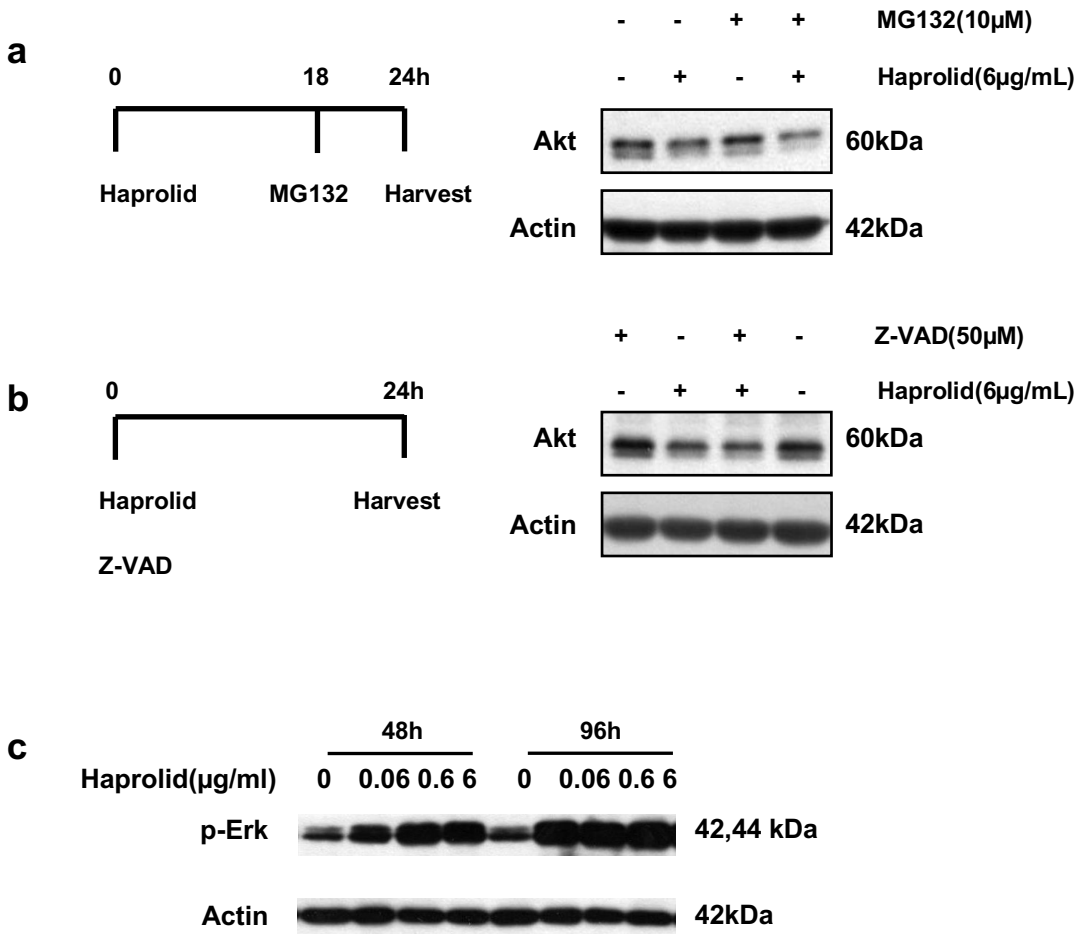

Figure 29. Haprolid-induced degradation of Akt protein is neither proteasome nor caspase dependent and Erk phosphorylation is significantly increased by Haprolid treatment. (a) Hep3B cells were treated with 6 μg/ml Haprolid for 24 hrs and 10 μM of the proteasome inhibitor MG132 (MG) were added to the samples 6 hrs before harvesting the cells. Whole-cell extracts were used to assess total Akt levels by immunoblotting. (b) Hep3B cells treated with 6 μg/ml Haprolid alone or in combination with 10 μM of a general caspase inhibitor, Z-VAD, for 24 hrs. Whole-cell extracts were used to evaluate total Akt protein level by immunoblotting. (c) Hep3B cells were treated with increasing concentrations of Haprolid for 48 hrs and 96 hrs. Cell lysates were analyzed by immunoblotting for p-Erk expression.

4. Discussion

Rb/E2F and Akt/mTOR pathways play a pivotal role in the molecular pathogenesis of HCC [43, 49, 53]. In this study, we report for the first time about the positive anti-tumor effect of Haprolid, a novel natural polyketide-peptide hybrid, in HCC models, both *in vitro* and *in vivo* through dual inbibition of Rb/E2F and Akt/mTOR pathways. We selected three representative human HCC cell lines: Hep3B, Huh-7 and HepG2. We found effective inhibition of cell growth in these cell lines. In addition, Hep3B cells demonstrated to be more sensitive to Haprolid treatment compared to Huh-7 and HepG2 cells.

In recent years, compelling evidence highlights the important role of EMT in the development of invasive and metastatic potentials of HCC progression and provides strong correlation with the prognosis of patients [82, 89, 90]. In this study, we demonstrate that Haprolid treatment reduces mesenchymal proteins such as N-cadherin, Vimentin and Snail expression in both Hep3B and Huh-7 cells. However, we only detect a subtle upregulation of epithelial marker E-cadherin, arguing for a selective control of EMT by Haprolid. Moreover, *in vitro* wound healing assays, Matrigel chamber assays and 3D tumor spheroid assays provide evidence that the cell motility and invasiveness are remarkably inhibited by Haprolid. These findings suggest that Haprolid has very good potential for attenuating EMT in HCC and could also be a promising strategy to suppress metastasis of HCC cells.

Relentless cell proliferation and compensatory suppression of apoptosis are ‘mission critical’ events which are required for the development of any and all cancers [91]. Adroit targeting of these critical events should have potent and

specific therapeutic consequences. As it was observed in our study, Haprolid treatment could strongly inhibit cell proliferation and negatively regulate the G1/S transition in HCC cells. Cell cycle analysis demonstrated that Haprolid significantly decreased cell population in S and G2-M phase. *In vitro* dynamic analysis revealed that Haprolid treatment induced strikingly decreased expression of both cyclin A and cyclin B. Fundamentally, cell-cycle transitions are strictly regulated by cyclins, which bind to and activate their catalytic partners, the CDKs [92, 93]. Cyclin A–CDK2 and cyclin A–CDK1 regulate the completion of S phase, whereas cyclin B–CDK1 is essential to take cells into mitosis [92]. In this view, the induction of cell cycle arrest by Haprolid is highly correlated with the inhibiton of these cyclins.

In addition, Hep3B cells presented a gradually increased population of sub-G1-phase cells under Haprolid treatment suggesting an induction of apoptosis. This was further substantiated by the Annexin V and PI staining which revealed that Haprolid treatment induced considerable apoptosis on Hep3B cells but not on Huh-7 and HepG2 cells. These findings indicate that induction of apoptosis is highly dependent on the concentration of the drugs as well as the individual susceptibility of the HCC cells. Indeed, extensive literature has disclosed that different HCC cell lines experienced different sensitivity to the induction of apoptosis [94-96]. In general, the growth inhibitory effect of Haprolid is mainly mediated by inhibition of cell proliferation, which is observed in the three tested cell lines to a similar extent. This reduction of proliferation is associated with a profound modulation of the expression of cell cycle mediators which leads to the cell cycle arrest and selectively induction of apoptosis.

The CDK-Rb-E2F pathway is a fundamental pathway in the control of cell cycle progression and proliferation [97, 98]. In the G1 phase, Rb is phosphorylated at low levels and associates with E2F transcription factors. Transcription is repressed until CDKs phosphorylate Rb and allow unrestrained E2F activity. E2F transcription factors then transcribe genes driving the G1/S cell cycle transition [44, 99]. We observed that Haprolid treatment effectively inhibited p-Rb and E2F-1 expressions in Huh-7 and HepG2 cells. Interestingly, Rb-deficient Hep3B cells also exhibited significant repression of E2F-1, suggesting that the potential involvement of other pocket proteins p107/p130 compensate for Rb loss, which has been reported by DB Rivadeneira et al. [100]. We hypothesize that in the Rb-deficient cells Haprolid might function on other pocket proteins p107/p130, whereas more evidents need to be further illustrated. Thus, these observations provided evidence that Haprolid induces growth arrest and apoptosis in HCC cells through interfering with the pocket protein/E2F signaling pathway. We also observed Haprolid treatment caused induction of p21 and p27 in Hep3B and HepG2 cells and p21 in Huh-7 cells. One of the reason to explain the discrepancy between Huh-7 and other tested HCC cells might due to the point mutation of p53 in Huh-7 cells at codon 220 [101]. It is known that the G1-checkpoint CDKIs - p21 and p27 conduct pivotal functions in cell cycle regulation via the coordination of internal and external signals that inhibit cell cycle progression [102]. Loss of expression or function of p21 and p27 has been implicated in the genesis or progression of many human malignancies [103]. Our data indicated that Haprolid suppresses growth of HCC cells *in vitro* through the induction of CDKIs and the inhibition of cyclins and CDKs.

As depicted in the results, we observed that Haprolid treatment demonstrated potent inhibition of p-Akt, p-mTOR, p-S6K and p-S6 expressions. Interestingly,

we also found that Haprolid inhibited Akt phosphorylation at high but increased signaling at low concentrations. In 2014 Breunig et al. [94] have demonstrated that HCC cell lines responded differentially to a group of BRaf and MEK Inhibitors depending on the concentration. Low-dose sorafenib treatment of HCC cells increased instead of decreased signaling. Inhibition of the MAPK (mitogen-activated protein kinase) pathway was only achieved by high drug concentrations. Strikely, we also found the downregulation of full form Akt. Although the expression level of total Akt is relativlely stable in cells, many studies have reported the changes of its level. In 2014, Choi et al. reported Salinomycin, a polyether ionophore antibiotic isolated from Streptomyces albus, could reduce of total Akt level and sensitized cancer cells to Akt inhibitor MK2206 [104]. In 2008, Mann et al. reported Arsenic trioxide which is used clinically to treat acute promyelocytic leukemia decreased total Akt protein in a caspase-dependent manner [105]. Adachi et al. described proteasome-dependent decrease in Akt by growth factors in vascular smooth muscle cells [106]. To further elaborate the mechanism of the downregulation of Akt we performed experiments by employing proteasome inhibitor MG132 and a pan caspase inhibitor Z-VAD. However, the reduction of total Akt level in Hep3B cells after Haprolid treatment is neither proteasome nor caspase dependent as depicted in Figure 29. Futhermore, since Ras/Erk pathway represents another dominant signaling in HCC tumorigenesis and there is a particularly intimate cross-talk between the PI3K/Akt and Ras/Erk pathways, where inhibitors of one pathway will often cause stimulation of the other [107]. In concordance with this consensus, we also determined a remarkable increase of Erk phosphorylation after Haprolid treatment as shown in Figure 29. These findings support the hypothesis that inhibiting only one of the signaling pathways may not be efficacious in HCC treatment, thus, promotes the strategy of inhibitor

combinations [108]. In summary, our study shows that Haprolid suppresses HCC carcinogenesis by interfering with the PI3K/Akt/mTOR signaling pathway. Therefore, this study provides support for Haprolid's anti-cancer effect.

The *in vivo* efficacy of Haprolid was examined using Hep3B cells grown as xenografts in nude mice. The observation that treatment of these tumor-bearing mice with Haprolid substantially impaired tumor development over a 5-week period without detectable side effects is both novel and of potential clinical relevance. Additionally, the IHC staining of tumor tissue sections demonstrates a lower expression of Ki-67, Akt and p-S6 after Haprolid treatment. These results are in accordance with our *in vitro* findings and further confirm the inhibition effect of Haprolid on proliferation and Akt signaling.

In conclusion, our results indicate that Haprolid treatment leads to a strong inhibitory effect of cell growth, migration and invasion in human HCC cell lines. This effect is linked with dual inhibition of Rb/E2F and Akt/mTOR pathway as well as repression of EMT. Cell cycle arrest and apoptosis also contribute to the growth inhibitory effect of Haprolid. Furthermore, we show that Haprolid also exhibits anti-tumor activity *in vivo* by using a HCC xenograft mouse model. Taken together, our observations highlight the possibility that Haprolid might be a new and promising candidate for therapy of HCC. Nevertheless, investigation of combination therapies of Haprolid and inhibitors of the RAF/MEK/ERK pathway, the tyrosine kinases (VEGFR, PDGFR), as well as combination with immune-checkpoint inhibitors are warranted in order to try to further extend the anti-tumor effect of Haprolid.

5. Summary

HCC represents a major health burden with limited curative treatment options. There is a pressing need for novel strategies to impact the progression of inoperable HCC. Haprolid is a novel natural product isolated from myxobacteria. Recent studies have reported Haprolid as a potent selective cytotoxin against a panel of tumor cells including HCC cells. The aims of the present study are to evaluate the efficacy of Haprolid in human HCC cell lines (Huh-7, Hep3B and HepG2) and xenograft tumors (NMRI-Foxn1^{nu} mice with injection of Hep3B cells) and to understand its underlying molecular mechanisms of action. Treatment with Haprolid significantly inhibited cell proliferation, migration and invasion *in vitro.* Haprolid impaired the epithelial-mesenchymal transition (EMT) through downregulation of N-cadherin, Vimentin and Snail. Moreover, growth of HCC cells *in vitro* was suppressed by inhibition of G1/S transition, and partially by induction of apoptosis. The drug induced downregulation of cell cycle regulatory proteins cyclin A, cyclin B and CDK2, and upregulation of p21 and p27. Further evidences showed that these effects of Haprolid were associated with Rb/E2F downregulation and Akt/mTOR inhibition. Finally, NMRI-Foxn1^{nu} xenografts treated by Haprolid resulted in significant tumor growth inhibition. Our results show for the first time, that Haprolid inhibits the growth of HCC both *in vitro* and *in vivo* through dual inbibition of Rb/E2F and Akt/mTOR pathways. Therefore, Haprolid might be considered as a new and promising candidate for the palliative therapy of HCC.

6. Zusammenfassung

Das hepatozelluäre Karzinom (HCC) ist ein zunehmender Tumor mit begrenzten kurativen Therapie Optionen. Neue Strategien sind erforderlich um die Tumorprogression des HCC aufzuhalten. Haprolid ist ein Naturstoff, welcher aus Myxobakterien isoliert wird. Studien haben gezeigt, dass Haprolid zytotoxische Eigenschaften besitzt und gegen Tumorzellen, einschließlich gegen das HCC wirkt. Ziele der aktuellen Arbeit sind die Effizienz von Haprolid an HCC Zelllinien (Huh-7, Hep3B, HepG2) und in einem Xenograft Modell (NMRI-Foxn1nu Mäuse mit Injektion von Hep3B Zellen) molekular zu untersuchen. Eine Therapie mit Haprolid inhibierte signifikant die Zellproliferation, Migration und Invasion in vitro. Haprolid beeinträchtigte die Epitheliale mesenchymale Transition (EMT) via Runterregulation von N-cadherin, Vimentin and Snail. Außerdem wurden HCC Zellen durch eine Inhibition der G1/S transition beeinträchtigt und es kam partiell zur Apoptose. Haprolid führte auch zu einer Runterregulation von Cyclin A, Cyclin B, CDK2, Rb/E2F, Akt/mTOR und zu einer Hochregulation von p21 und p27. Haprolid inhibierte signifikant das Wachstum von NMRI-Foxn1nu Xenograft Tumore. Unsere Ergebnisse zeigen erstmalig, dass Haprolid das Wachstum des HCC in vitro und in vivo durch eine Inhibition des Rb/E2F und Akt/mTOR Signalwegs einschränken kann. Haprolid stellt daher eine neue und erfolgsversprechende Substanz zur palliative Therapie des HCC dar.

7. Bibliography

1. Bray, F., et al., *Global cancer statistics 2018: GLOBOCAN estimates of incidence and mortality worldwide for 36 cancers in 185 countries.* CA Cancer J Clin, 2018. **68**(6): p. 394-424.
2. Llovet, J.M., et al., *Hepatocellular carcinoma.* Nat Rev Dis Primers, 2016. **2**: p. 16018.
3. Petrick, J.L., et al., *Future of Hepatocellular Carcinoma Incidence in the United States Forecast Through 2030.* J Clin Oncol, 2016. **34**(15): p. 1787-94.
4. Gerbes, A., et al., *Gut roundtable meeting paper: selected recent advances in hepatocellular carcinoma.* Gut, 2018. **67**(2): p. 380-388.
5. (IARC), T.I.A.f.R.o.C. *Globocan 2018*. Available from: http://gco.iarc.fr/today/fact-sheets-cancers
6. Sia, D., et al., *Liver Cancer Cell of Origin, Molecular Class, and Effects on Patient Prognosis.* Gastroenterology, 2017. **152**(4): p. 745-761.
7. Collaboration, G.B.o.D.L.C., *The Burden of Primary Liver Cancer and Underlying Etiologies From 1990 to 2015 at the Global, Regional, and National Level: Results From the Global Burden of Disease Study 2015The Global Burden of Liver Cancer 2015The Global Burden of Liver Cancer 2015.* JAMA Oncology, 2017. **3**(12): p. 1683-1691.
8. Frazier, T.H., et al., *Treatment of alcoholic liver disease.* Therap Adv Gastroenterol, 2011. **4**(1): p. 63-81.
9. Massarweh, N.N. and H.B. El-Serag, *Epidemiology of Hepatocellular Carcinoma and Intrahepatic Cholangiocarcinoma.* Cancer Control, 2017. **24**(3): p. 1073274817729245.
10. Argyrou, C., D. Moris, and S. Vernadakis, *Hepatocellular carcinoma development in non-alcoholic fatty liver disease and non-alcoholic steatohepatitis. Is it going to be the "Plague" of the 21st century? A literature review focusing on pathogenesis, prevention and treatment.* J buon, 2017. **22**(1): p. 6-20.
11. Asrani, S.K., et al., *Burden of liver diseases in the world.* Journal of Hepatology, 2019. **70**(1): p. 151-171.
12. Bugianesi, E., *Non-alcoholic steatohepatitis and cancer.* Clin Liver Dis, 2007. **11**(1): p. 191-207, x-xi.
13. Dyson, J., et al., *Hepatocellular cancer: the impact of obesity, type 2 diabetes and a multidisciplinary team.* J Hepatol, 2014. **60**(1): p. 110-7.
14. Kanwal, F., et al., *Trends in the Burden of Nonalcoholic Fatty Liver Disease in a United States Cohort of Veterans.* Clin Gastroenterol Hepatol, 2016. **14**(2): p. 301-8.e1-2.

15. Younossi, Z.M., et al., *Association of nonalcoholic fatty liver disease (NAFLD) with hepatocellular carcinoma (HCC) in the United States from 2004 to 2009.* Hepatology, 2015. **62**(6): p. 1723-30.
16. Hagstrom, H., P. Tynelius, and F. Rasmussen, *High BMI in late adolescence predicts future severe liver disease and hepatocellular carcinoma: a national, population-based cohort study in 1.2 million men.* Gut, 2018. **67**(8): p. 1536-1542.
17. Kew, M.C., *Aflatoxins as a cause of hepatocellular carcinoma.* J Gastrointestin Liver Dis, 2013. **22**(3): p. 305-10.
18. Hsu, I.C., et al., *Mutational hotspot in the p53 gene in human hepatocellular carcinomas.* Nature, 1991. **350**(6317): p. 427-8.
19. Massoud, O. and M. Charlton, *Nonalcoholic Fatty Liver Disease/Nonalcoholic Steatohepatitis and Hepatocellular Carcinoma.* Clin Liver Dis, 2018. **22**(1): p. 201-211.
20. Sangiovanni, A., et al., *The natural history of compensated cirrhosis due to hepatitis C virus: A 17-year cohort study of 214 patients.* Hepatology, 2006. **43**(6): p. 1303-10.
21. Malek, N.P., et al., *The diagnosis and treatment of hepatocellular carcinoma.* Dtsch Arztebl Int, 2014. **111**(7): p. 101-6.
22. Marrero, J.A., et al., *Diagnosis, Staging, and Management of Hepatocellular Carcinoma: 2018 Practice Guidance by the American Association for the Study of Liver Diseases.* Hepatology, 2018. **68**(2): p. 723-750.
23. Vogel, A., et al., *Hepatocellular carcinoma: ESMO Clinical Practice Guidelines for diagnosis, treatment and follow-up.* Ann Oncol, 2018. **29**(Supplement_4): p. iv238-iv255.
24. Llovet, J.M., et al., *Sorafenib in advanced hepatocellular carcinoma.* N Engl J Med, 2008. **359**(4): p. 378-90.
25. Matsui, J., et al., *Multi-kinase inhibitor E7080 suppresses lymph node and lung metastases of human mammary breast tumor MDA-MB-231 via inhibition of vascular endothelial growth factor-receptor (VEGF-R) 2 and VEGF-R3 kinase.* Clin Cancer Res, 2008. **14**(17): p. 5459-65.
26. Wilhelm, S.M., et al., *Regorafenib (BAY 73-4506): a new oral multikinase inhibitor of angiogenic, stromal and oncogenic receptor tyrosine kinases with potent preclinical antitumor activity.* Int J Cancer, 2011. **129**(1): p. 245-55.
27. Nault, J.C. and J. Zucman-Rossi, *Genetics of hepatocellular carcinoma: the next generation.* J Hepatol, 2014. **60**(1): p. 224-6.
28. Zhu, A.X., et al., *HCC and angiogenesis: possible targets and future directions.* Nat Rev Clin Oncol, 2011. **8**(5): p. 292-301.

29. Meguro, M., et al., *The molecular pathogenesis and clinical implications of hepatocellular carcinoma.* Int J Hepatol, 2011. **2011**: p. 818672.
30. Pinter, M. and M. Peck-Radosavljevic, *Review article: systemic treatment of hepatocellular carcinoma.* Aliment Pharmacol Ther, 2018. **48**(6): p. 598-609.
31. Zucman-Rossi, J., et al., *Genetic Landscape and Biomarkers of Hepatocellular Carcinoma.* Gastroenterology, 2015. **149**(5): p. 1226-1239.e4.
32. Avila, M.A., et al., *New therapies for hepatocellular carcinoma.* Oncogene, 2006. **25**(27): p. 3866-84.
33. Cavenee, W.K., et al., *Expression of recessive alleles by chromosomal mechanisms in retinoblastoma.* Nature, 1983. **305**(5937): p. 779-84.
34. Knudson, A.G., Jr., *Mutation and cancer: statistical study of retinoblastoma.* Proc Natl Acad Sci U S A, 1971. **68**(4): p. 820-3.
35. Weinberg, R.A., *Tumor suppressor genes.* Science, 1991. **254**(5035): p. 1138-46.
36. Yunis, J.J. and N. Ramsay, *Retinoblastoma and subband deletion of chromosome 13.* Am J Dis Child, 1978. **132**(2): p. 161-3.
37. Buchkovich, K., L.A. Duffy, and E. Harlow, *The retinoblastoma protein is phosphorylated during specific phases of the cell cycle.* Cell, 1989. **58**(6): p. 1097-105.
38. Chen, P.L., et al., *Phosphorylation of the retinoblastoma gene product is modulated during the cell cycle and cellular differentiation.* Cell, 1989. **58**(6): p. 1193-8.
39. DeCaprio, J.A., et al., *The product of the retinoblastoma susceptibility gene has properties of a cell cycle regulatory element.* Cell, 1989. **58**(6): p. 1085-95.
40. Chellappan, S.P., et al., *The E2F transcription factor is a cellular target for the RB protein.* Cell, 1991. **65**(6): p. 1053-61.
41. Nevins, J.R., *E2F: a link between the Rb tumor suppressor protein and viral oncoproteins.* Science, 1992. **258**(5081): p. 424-9.
42. Weintraub, S.J., C.A. Prater, and D.C. Dean, *Retinoblastoma protein switches the E2F site from positive to negative element.* Nature, 1992. **358**(6383): p. 259-61.
43. Llovet, J.M. and J. Bruix, *Molecular targeted therapies in hepatocellular carcinoma.* Hepatology, 2008. **48**(4): p. 1312-27.
44. Dick, F.A. and S.M. Rubin, *Molecular mechanisms underlying RB protein function.* Nat Rev Mol Cell Biol, 2013. **14**(5): p. 297-306.
45. Manning, A.L., et al., *Suppression of genome instability in pRB-deficient cells by enhancement of chromosome cohesion.* Mol Cell, 2014. **53**(6): p. 993-1004.

46. Sherr, C.J., *Cancer cell cycles.* Science, 1996. **274**(5293): p. 1672-7.
47. Narasimha, A.M., et al., *Cyclin D activates the Rb tumor suppressor by mono-phosphorylation.* Elife, 2014. **3**.
48. Yao, G., et al., *A bistable Rb-E2F switch underlies the restriction point.* Nat Cell Biol, 2008. **10**(4): p. 476-82.
49. Sherr, C.J. and F. McCormick, *The RB and p53 pathways in cancer.* Cancer Cell, 2002. **2**(2): p. 103-12.
50. Bellacosa, A., et al., *A retroviral oncogene, akt, encoding a serine-threonine kinase containing an SH2-like region.* Science, 1991. **254**(5029): p. 274-7.
51. Coffer, P.J. and J.R. Woodgett, *Molecular cloning and characterisation of a novel putative protein-serine kinase related to the cAMP-dependent and protein kinase C families.* Eur J Biochem, 1991. **201**(2): p. 475-81.
52. Jones, P.F., et al., *Molecular cloning and identification of a serine/threonine protein kinase of the second-messenger subfamily.* Proc Natl Acad Sci U S A, 1991. **88**(10): p. 4171-5.
53. Manning, B.D. and A. Toker, *AKT/PKB Signaling: Navigating the Network.* Cell, 2017. **169**(3): p. 381-405.
54. Ersahin, T., N. Tuncbag, and R. Cetin-Atalay, *The PI3K/AKT/mTOR interactive pathway.* Mol Biosyst, 2015. **11**(7): p. 1946-54.
55. Nakanishi, K., et al., *Akt phosphorylation is a risk factor for early disease recurrence and poor prognosis in hepatocellular carcinoma.* Cancer, 2005. **103**(2): p. 307-12.
56. Schmitz, K.J., et al., *Activation of the ERK and AKT signalling pathway predicts poor prognosis in hepatocellular carcinoma and ERK activation in cancer tissue is associated with hepatitis C virus infection.* J Hepatol, 2008. **48**(1): p. 83-90.
57. Golob-Schwarzl, N., et al., *New liver cancer biomarkers: PI3K/AKT/mTOR pathway members and eukaryotic translation initiation factors.* Eur J Cancer, 2017. **83**: p. 56-70.
58. LoPiccolo, J., et al., *Targeting the PI3K/Akt/mTOR pathway: effective combinations and clinical considerations.* Drug Resist Updat, 2008. **11**(1-2): p. 32-50.
59. Alessi, D.R., et al., *Mechanism of activation of protein kinase B by insulin and IGF-1.* Embo j, 1996. **15**(23): p. 6541-51.
60. Alessi, D.R., et al., *Characterization of a 3-phosphoinositide-dependent protein kinase which phosphorylates and activates protein kinase Balpha.* Curr Biol, 1997. **7**(4): p. 261-9.
61. Stokoe, D., et al., *Dual role of phosphatidylinositol-3,4,5-trisphosphate in the activation of protein kinase B.* Science, 1997. **277**(5325): p. 567-70.

62. Sarbassov, D.D., et al., *Phosphorylation and regulation of Akt/PKB by the rictor-mTOR complex.* Science, 2005. **307**(5712): p. 1098-101.
63. Yang, J., et al., *Crystal structure of an activated Akt/protein kinase B ternary complex with GSK3-peptide and AMP-PNP.* Nat Struct Biol, 2002. **9**(12): p. 940-4.
64. Cross, D.A., et al., *Inhibition of glycogen synthase kinase-3 by insulin mediated by protein kinase B.* Nature, 1995. **378**(6559): p. 785-9.
65. Ding, Q., et al., *Degradation of Mcl-1 by beta-TrCP mediates glycogen synthase kinase 3-induced tumor suppression and chemosensitization.* Mol Cell Biol, 2007. **27**(11): p. 4006-17.
66. Maurer, U., et al., *Glycogen synthase kinase-3 regulates mitochondrial outer membrane permeabilization and apoptosis by destabilization of MCL-1.* Mol Cell, 2006. **21**(6): p. 749-60.
67. Morel, C., et al., *Mcl-1 integrates the opposing actions of signaling pathways that mediate survival and apoptosis.* Mol Cell Biol, 2009. **29**(14): p. 3845-52.
68. Sears, R., et al., *Multiple Ras-dependent phosphorylation pathways regulate Myc protein stability.* Genes Dev, 2000. **14**(19): p. 2501-14.
69. Welcker, M., et al., *The Fbw7 tumor suppressor regulates glycogen synthase kinase 3 phosphorylation-dependent c-Myc protein degradation.* Proc Natl Acad Sci U S A, 2004. **101**(24): p. 9085-90.
70. Kaidanovich-Beilin, O. and J.R. Woodgett, *GSK-3: Functional Insights from Cell Biology and Animal Models.* Front Mol Neurosci, 2011. **4**: p. 40.
71. van der Vos, K.E. and P.J. Coffer, *The extending network of FOXO transcriptional target genes.* Antioxid Redox Signal, 2011. **14**(4): p. 579-92.
72. Webb, A.E. and A. Brunet, *FOXO transcription factors: key regulators of cellular quality control.* Trends Biochem Sci, 2014. **39**(4): p. 159-69.
73. Brunet, A., et al., *Akt promotes cell survival by phosphorylating and inhibiting a Forkhead transcription factor.* Cell, 1999. **96**(6): p. 857-68.
74. Kops, G.J., et al., *Direct control of the Forkhead transcription factor AFX by protein kinase B.* Nature, 1999. **398**(6728): p. 630-4.
75. Saxton, R.A. and D.M. Sabatini, *mTOR Signaling in Growth, Metabolism, and Disease.* Cell, 2017. **168**(6): p. 960-976.
76. Inoki, K., et al., *TSC2 is phosphorylated and inhibited by Akt and suppresses mTOR signalling.* Nat Cell Biol, 2002. **4**(9): p. 648-57.
77. Manning, B.D., et al., *Identification of the tuberous sclerosis complex-2 tumor suppressor gene product tuberin as a target of the phosphoinositide 3-kinase/akt pathway.* Mol Cell, 2002. **10**(1): p. 151-62.
78. Potter, C.J., L.G. Pedraza, and T. Xu, *Akt regulates growth by directly phosphorylating Tsc2.* Nat Cell Biol, 2002. **4**(9): p. 658-65.

79. Nave, B.T., et al., *Mammalian target of rapamycin is a direct target for protein kinase B: identification of a convergence point for opposing effects of insulin and amino-acid deficiency on protein translation.* Biochem J, 1999. **344 Pt 2**: p. 427-31.
80. Sekulic, A., et al., *A direct linkage between the phosphoinositide 3-kinase-AKT signaling pathway and the mammalian target of rapamycin in mitogen-stimulated and transformed cells.* Cancer Res, 2000. **60**(13): p. 3504-13.
81. Steinmetz, H., et al., *Isolation, Structure Elucidation, and (Bio)Synthesis of Haprolid, a Cell-Type-Specific Myxobacterial Cytotoxin.* Angew Chem Int Ed Engl, 2016. **55**(34): p. 10113-7.
82. Giannelli, G., et al., *Role of epithelial to mesenchymal transition in hepatocellular carcinoma.* J Hepatol, 2016. **65**(4): p. 798-808.
83. Kalluri, R. and R.A. Weinberg, *The basics of epithelial-mesenchymal transition.* J Clin Invest, 2009. **119**(6): p. 1420-8.
84. Cano, A., et al., *The transcription factor snail controls epithelial-mesenchymal transitions by repressing E-cadherin expression.* Nat Cell Biol, 2000. **2**(2): p. 76-83.
85. Oliver, F.J., et al., *Importance of poly(ADP-ribose) polymerase and its cleavage in apoptosis. Lesson from an uncleavable mutant.* J Biol Chem, 1998. **273**(50): p. 33533-9.
86. Nevins, J.R., *The Rb/E2F pathway and cancer.* Hum Mol Genet, 2001. **10**(7): p. 699-703.
87. Dufner, A., et al., *Protein kinase B localization and activation differentially affect S6 kinase 1 activity and eukaryotic translation initiation factor 4E-binding protein 1 phosphorylation.* Mol Cell Biol, 1999. **19**(6): p. 4525-34.
88. Peterson, R.T., et al., *FKBP12-rapamycin-associated protein (FRAP) autophosphorylates at serine 2481 under translationally repressive conditions.* J Biol Chem, 2000. **275**(10): p. 7416-23.
89. Kodama, T., et al., *Transposon mutagenesis identifies genes and cellular processes driving epithelial-mesenchymal transition in hepatocellular carcinoma.* Proc Natl Acad Sci U S A, 2016. **113**(24): p. E3384-93.
90. Mir, N., et al., *Epithelial-to-Mesenchymal Transition: A Mediator of Sorafenib Resistance in Advanced Hepatocellular Carcinoma.* Curr Cancer Drug Targets, 2017. **17**(8): p. 698-706.
91. Evan, G.I. and K.H. Vousden, *Proliferation, cell cycle and apoptosis in cancer.* Nature, 2001. **411**(6835): p. 342-8.
92. Hochegger, H., S. Takeda, and T. Hunt, *Cyclin-dependent kinases and cell-cycle transitions: does one fit all?* Nat Rev Mol Cell Biol, 2008. **9**(11): p. 910-6.

93. Hydbring, P., M. Malumbres, and P. Sicinski, *Non-canonical functions of cell cycle cyclins and cyclin-dependent kinases.* Nat Rev Mol Cell Biol, 2016. **17**(5): p. 280-92.
94. Breunig, C., et al., *BRaf and MEK inhibitors differentially regulate cell fate and microenvironment in human hepatocellular carcinoma.* Clin Cancer Res, 2014. **20**(9): p. 2410-23.
95. Liu, C.Y., et al., *An indolylquinoline derivative activates DNA damage response and apoptosis in human hepatocellular carcinoma cells.* Int J Oncol, 2016. **49**(6): p. 2431-2441.
96. Herzer, K., et al., *IFN-alpha-induced apoptosis in hepatocellular carcinoma involves promyelocytic leukemia protein and TRAIL independently of p53.* Cancer Res, 2009. **69**(3): p. 855-62.
97. Calzone, L., et al., *A comprehensive modular map of molecular interactions in RB/E2F pathway.* Mol Syst Biol, 2008. **4**: p. 173.
98. Harbour, J.W. and D.C. Dean, *The Rb/E2F pathway: expanding roles and emerging paradigms.* Genes Dev, 2000. **14**(19): p. 2393-409.
99. Evangelou, K., S. Havaki, and A. Kotsinas, *E2F transcription factors and digestive system malignancies: how much do we know?* World J Gastroenterol, 2014. **20**(29): p. 10212-6.
100. Rivadeneira, D.B., et al., *Proliferative suppression by CDK4/6 inhibition: complex function of the retinoblastoma pathway in liver tissue and hepatoma cells.* Gastroenterology, 2010. **138**(5): p. 1920-1930.
101. Hsu, I.C., et al., *p53 gene mutation and integrated hepatitis B viral DNA sequences in human liver cancer cell lines.* Carcinogenesis, 1993. **14**(5): p. 987-92.
102. Li, W., et al., *The role of cell cycle regulatory proteins in the pathogenesis of melanoma.* Pathology, 2006. **38**(4): p. 287-301.
103. Abukhdeir, A.M. and B.H. Park, *P21 and p27: roles in carcinogenesis and drug resistance.* Expert Rev Mol Med, 2008. **10**: p. e19.
104. Choi, A.R., J.H. Kim, and S. Yoon, *Corrigendum to "Sensitization of Cancer Cells through Reduction of Total Akt and Downregulation of Salinomycin-Induced pAkt, pGSk3 beta , pTSC2, and p4EBP1 by Cotreatment with MK-2206".* Biomed Res Int, 2015. **2015**: p. 138260.
105. Mann, K.K., M. Colombo, and W.H. Miller, Jr., *Arsenic trioxide decreases AKT protein in a caspase-dependent manner.* Mol Cancer Ther, 2008. **7**(6): p. 1680-7.
106. Adachi, M., et al., *Proteasome-dependent decrease in Akt by growth factors in vascular smooth muscle cells.* FEBS Lett, 2003. **554**(1-2): p. 77-80.

107. Mendoza, M.C., E.E. Er, and J. Blenis, *The Ras-ERK and PI3K-mTOR pathways: cross-talk and compensation.* Trends Biochem Sci, 2011. **36**(6): p. 320-8.
108. Gedaly, R., et al., *The role of PI3K/mTOR inhibition in combination with sorafenib in hepatocellular carcinoma treatment.* Anticancer Res, 2012. **32**(7): p. 2531-6.

8. Declaration of Contributions

The dissertation work was carried out at the University Hospital Tübingen under the supervision of Prof. Dr. med Ruben R. Plentz. The study was designed by Prof. Dr. med Ruben R. Plentz. After training by laboratory members, I carried out all experiments independently. Statistical analysis was carried out independently by myself.

I confirm that I wrote the manuscript myself and that any additional sources of information have been duly cited.

……..(Signature)……. (Place/Date)

9. Acknowledgments

Firstly, I would like to express my sincere gratitude to my supervisor Prof. Dr. med. Ruben R. Plentz for the continuous support of my work, for his patience, motivation, and immense knowledge. He is always very enthusiastic, optimistic and supportive.

A very special gratitude goes to Prof. Nisar P. Malek and Dr. Przemyslaw Bozko for their tremendous help during my work. Meanwhile, I would like to thank Prof. Markus Kalesse and Prof. Marc Stadler for very kindly providing us the compound and sharing their knowledge. I am also very grateful to Prof. Ludwig Wilkens for his professional help regarding to the pathological analysis.

In particular, I thank my fellow labmates Vikas Bhuria, Khac Cuong Bui and Mai Ly Thi Nguyen for the stimulating discussions and sharing their knowledge during my experiment. I greatly appreciate Dr. Chih-Jen Hsieh and Zexi, Hu for their great and continuous support in both professional and personal life. Many thanks to Mathias, Sebastian, Louise, Christine, Tim and Hilde for their precious supports.

Last but not the least, I would like to thank my family and my friends for their endless love and supports which are always with me in my life.